A single-layer urban canopy model with transmissive radiation exchange between trees and street canyons

Chenghao Wang[a,*], Zhi-Hua Wang[b], Young-Hee Ryu[c]

[a] *Department of Earth System Science, Stanford University, Stanford, CA 94305, USA*

[b] *School of Sustainable Engineering and the Built Environment, Arizona State University, Tempe, AZ 85287, USA*

[c] *Division of Environmental Science and Engineering, Pohang University of Science and Technology, Pohang, 37673, South Korea*

[*] Corresponding author. E-mail address: chenghao.wang@stanford.edu. Tel: +1-480-616-8910.

Abstract

Urban trees are one of the most effective strategies to mitigate excessive heat stress in cities. To understand the underlying mechanisms of their cooling effect and to assess their use in urban planning, the accurate simulation of how trees interact with the ambient built environment is critical and imperative. However, the representation of urban trees in existing urban canopy models (in particular single-layer ones) remains oversimplified. Here we develop a new Monte Carlo ray tracing method to explicitly resolve the canopy transmittance and evaluate its impact on radiative view factors between trees and regular building facets. The new method is highly accurate in reproducing analytical solutions. Sensitivity tests of radiative view factors suggest the importance of canopy transmittance in changing the radiation exchange. We then incorporate the ray tracing algorithm into the new version of the Arizona State University (ASU) Single-Layer Urban Canopy Model (ASLUM v3.1). In addition to radiation transmittance, ASLUM v3.1 explicitly resolves the radiative shading, evapotranspiration, and root water uptake of urban trees in street canyons, with significantly improved performance in predictions (especially latent heat flux) when compared to previous versions. We further apply ASLUM v3.1 to evaluate the impacts of trees with varying characteristics on urban radiation exchange and turbulent heat fluxes. Results show that urban trees reduce the net radiation of ground and wall as well as the daytime temperature via shading and transpiration, but may slightly warm the nighttime street canyons through radiative trapping effect.

Keywords:

Urban trees; urban canopy model; Monte Carlo ray tracing; canopy transmittance; view factors; cooling effect

1. Introduction

Urban trees are one of the most effective and versatile nature-based solutions to improve environmental quality in cities. Especially, they alleviate daytime excessive urban heat stress during hot summers mainly through radiative shading and evapotranspiration [1]. The cooling effect of urban trees has been assessed and demonstrated in numerous field experiments and studies based on remote sensing techniques [2–5]. They are also found to efficiently improve the pedestrian thermal comfort, reduce the building energy consumption for cooling, and offset carbon emissions [6–9]. On the other hand, the efficacy of urban trees depends on many factors such as synoptic weather conditions, background climates, and tree species. Assessment is therefore necessary prior to and during the implementation of trees in urban planning and design, during which accurate numerical models are needed.

Extensive efforts have been made to improve urban tree modeling in micro- and local-scale numerical simulations during the past two decades. The simplest models include semi-analytical or empirical ones and those simulate trees (and other vegetation) as a separate tile. For example, Shashua-Bar and Hoffman [10] developed an empirical model (Green CTTC) and evaluated the cooling effect of urban trees as the shading partially offset by the convective heat exchange. The Surface Urban Energy and Water Balance Scheme (SUEWS) proposed by Järvi et al. [11] simulates the energy and water exchange of urban deciduous and coniferous trees as individual surface types parallel to paved surfaces and buildings. In contrast, urban canopy models address the impacts of urban geometry using the simplified two-dimensional (2D) street canyon representation [12–14], in which trees are usually modeled as a single layer [15,16], opaque elements [17–19], or porous media [20,21]. Several urban canopy models have been coupled with atmospheric models to investigate how urban trees affect the regional and mesoscale land–atmosphere exchange processes [22–26]. For instance, Loughner et al. [22] and Lee et al. [23] implemented the Vegetated Urban Canopy Model (VUCM) [16] into the mesoscale Weather Research and Forecasting (WRF) model and assessed the cooling effect of urban trees in Washington–Baltimore metropolitan area and Seoul metropolitan area, respectively. Similarly, Upreti et al. [24] and Wang et al. [25] coupled a single-layer urban canopy model [27] to the WRF model to examine the impacts of shade trees on temperatures, surface energy partitioning, and human thermal comfort in the Phoenix metropolitan area and the contiguous United States, respectively. Computational fluid dynamics (CFD) models represent another model category that solves the exchange of mass, momentum, and energy between building surfaces and trees, albeit with high computational cost [28–36]. In particular, the impact of trees (as porous media) on the flow field is usually modeled as a source term in the momentum equation [29,31–33,35]. ENVI-met is probably one of the most widely used fine-scale CFD-based tools to model urban trees, although it requires detailed urban morphological input for the study area [30,34,37,38].

Realistically resolving vegetation (including trees) is critical to modeling urban surface energy exchange [39]. Compared to empirical, slab, and CFD models, urban canopy models are capable of simulating physical processes influenced by common 2D urban structure and trees with intermediate complexity. Urban canopy models can be broadly categorized into single-layer and multilayer models [40]. Among single-layer urban canopy models, the VUCM [16] is one of the earliest ones that consider trees, in which the energy balance of trees is modeled using the big leaf approach. Using a Monte Carlo ray tracing method, Wang's [17] model exclusively simulates the radiative shading effect of urban trees in a single-layer urban canopy model [27]. This model is reintroduced here as the Arizona State University (ASU) Single-Layer Urban

Canopy Model (ASLUM) v3.0 (see details in Section 2). The same ray tracing method was later adopted in the urban canopy model proposed by Ryu et al. [18]. Ryu et al.'s [18] model explicitly resolves the shading, transpiration, and root water uptake of urban trees. The Town Energy Balance (TEB) model has been refined to simulate the influence of urban trees on urban radiation exchange and airflow (TEB-SURFEX) [41]. Recently, the ecohydrological dynamics of urban trees were incorporated into the Urban Tethys-Chloris (UT&C) model proposed by Meili et al. [19]. Urban trees have also been included in a multilayer urban canopy model (BEP-tree) to evaluate their impacts on pedestrian-level micrometeorology, although this model does not include hydrological modules [20,21].

It is noteworthy that radiative view factors are one of the key components in resolving the shortwave and longwave radiation budget in urban canopy models [12,14], especially those with trees integrated. However, due to the complex three-dimensional (3D) nature of trees, the accurate modeling of the impact of trees on view factors is challenging. Among the single-layer family, the VUCM [16] and TEB-SURFEX [15,41] use analytically derived view factors for street canyons without trees, while the impact of trees is implicitly considered with transmissivities as ad hoc reduction factors. In contrast, the current version of ASLUM [17], Ryu et al.'s [18] model, and UT&C model [19] simulate view factors using the Monte Carlo ray tracing approach. The Monte Carlo ray tracing approach can numerically determine the view factors and radiation exchange between various (complex) surfaces using randomized energy bundles [42]. Nevertheless, in existing single-layer urban canopy models with ray tracing methods, trees are assumed to be opaque with no canopy gap fraction (gaps between leaves within tree crowns) [17–19]. Similar assumption has been made in those based on analytical view factors as well (e.g., the TUrban model [43]), which may induce large errors for sparse tree canopy. In addition, the validation of view factors between trees and street canyon facets remains relatively rare, primarily due to the lack of measurements.

The objective of this study is twofold: (1) to develop a new Monte Carlo ray tracing method that explicitly incorporates the transmittance of foliage, and (2) to develop a new version of ASLUM (v3.1) that can simulate both radiative shading and evapotranspiration of urban trees (cf. only shading in ASLUM v3.0 [17]). The proposed models are expected to improve the representation of trees in the current versions of ASLUM and other urban canopy models. We first review the history of three generations of ASLUM in Section 2. The details of new models are introduced in Section 3. We then evaluate the performance of the proposed models with analytical solutions and field measurements (Sections 4.1, 4.2, and 4.5). In particular, the sensitivity of radiative view factors to geometry and canopy transmittance is thoroughly evaluated in Sections 4.3 and 4.4. We also apply the new ASLUM to simulate the cooling effect of trees with varying characteristics in Section 5.

2. Arizona State University Single-Layer Urban Canopy Model (ASLUM)

The **A**rizona State University **S**ingle-**L**ayer **U**rban Canopy **M**odel (ASLUM) is a local/neighborhood-scale urban canopy model that physically resolves multiple processes (including the exchanges of heat, mass, and momentum) within the urban canopy layer. It represents the urban canopy layer as an infinitely long "big canyon" (2D) with specific dimensions and orientation [12,13]. ASLUM has undergone a decade of continuous development since ~2011 (see Table 1 and Fig. 1), and it is also among the earlier single-layer urban canopy models that explicitly resolve subfacet heterogeneity [44,45].

Table 1. Three generations of ASU Single-Layer Urban Canopy Model with major features.

Version	Major features	Key references
ASLUM v1.x	Basic urban energy and momentum exchanges; subfacet heterogeneity; Green's function-based surface temperatures and conductive heat fluxes	[44,46–48]
ASLUM v2.x	Detailed ground vegetation (grass) and roof vegetation (green roof); hydrological components; urban irrigation; anthropogenic heat; urban oasis effect	[27,49–51]
ASLUM v3.x	Trees (radiative shading, evapotranspiration, and root water uptake)	[8,17] and the present study

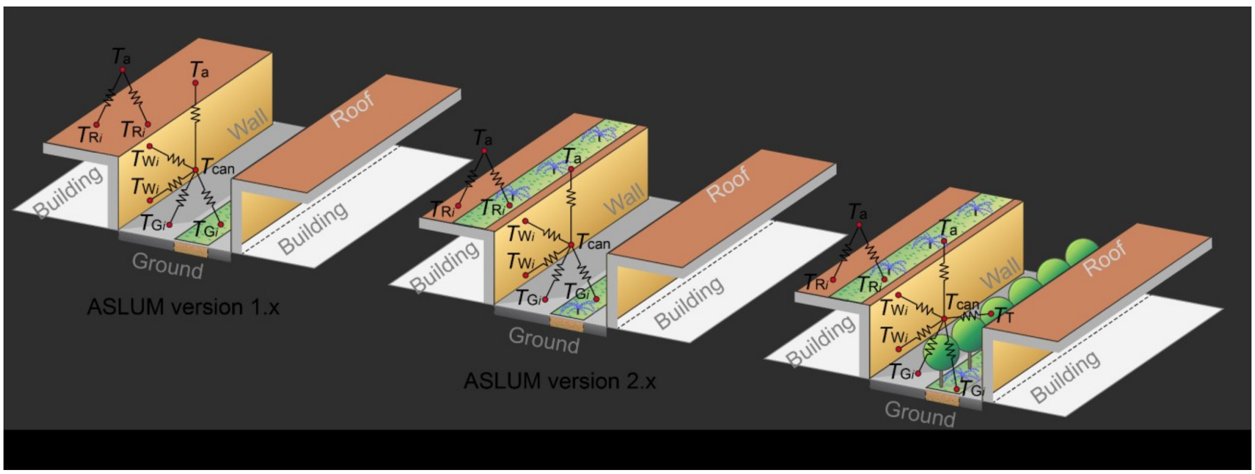

Figure 1. Schematic structures of three generations of the Arizona State University Single-Layer Urban Canopy Model with resistance networks of energy transport. *T* is temperature, with subscripts a, can, R, W, G, and T denoting air, canyon air, roof, wall, ground, and tree, respectively. The subscript *i* denotes different types of subfacets.

(Figure 1 is a 2-column fitting image)

The first generation of ASLUM (v1.x) is developed based upon the offline version of the single-layer urban canopy model in the Weather Research and Forecasting (WRF) model [13,52]. Besides basic energy and momentum exchanges, ASLUM v1.x permits heterogeneity on each urban facet (walls, ground, and roof) [44]. For example, roofs can be a combination of conventional roofs and green roofs; ground surfaces can be composed of asphalt, concrete, bare soil, and ground vegetation (e.g., lawns); wall surfaces can consist of brick and glass. In addition, ASLUM v1.x analytically resolves surface temperatures and conductive heat fluxes for solid media (walls, ground, roof, and soil) based on the Green's function approach [46–48]. The second generation of ASLUM (v2.x) features detailed ground and roof vegetation modeling [27], including a multi-layer green roof system [49–51]. ASLUM v2.x contains hydrological components to prognostically resolve soil moisture dynamics and evapotranspiration/evaporation from both natural surfaces and engineered surfaces (via a water-holding layer [27]). It incorporates some urban metabolic activities such as urban irrigation and anthropogenic heat fluxes [50]. ASLUM v2.x can also simulate the oasis effect on urban vegetation evapotranspiration [50]. The major improvement of the third generation of ASLUM (v3.x) is the numerical representation of urban trees. ASLUM v3.0 implicitly simulates the radiative shading effect of street trees via changes in radiative view factors based on a Monte Carlo ray tracing method [17]. This concise representation of urban trees enables the evaluation of the cooling effect and energy savings due to shade trees [8], but other complicated biophysical functions of urban trees (e.g., transpiration and root water uptake) are not resolved in v3.0.

Three generations of ASLUM have been extensively evaluated against field measurements with diverse background climates, showing good performance of reproducing different processes within the urban canopy layer (e.g., [24,27,47,50]). The sensitivity of the ASLUM to input parameters has been thoroughly evaluated using an advanced Monte Carlo simulation approach (subset simulation) (e.g., [44]). ASLUM has also been used to assess the efficacy (e.g., cooling, thermal comfort, and energy saving) of various urban heat mitigation strategies, such as white roofs, green roofs, lawns, trees, and urban irrigation (e.g., [8,17,50,53]). ASLUM is capable of being coupled to atmospheric models to simulate urban land–atmosphere interactions. ASLUM v2.x and v3.0 has been coupled to the WRF model for regional and continental scales simulations (e.g., [24,25,54]). In particular, ASLUM v2.x has been included in the public releases of the WRF model [50,55]. In addition, ASLUM v2.x and v3.0 have been coupled with a single column atmospheric model to extend the evaluation of urban heat mitigation strategies to the entire urban boundary layer (e.g., [56]).

In this study, we develop ASLUM v3.1 primarily based upon ASLUM v3.0 [8,17] and Ryu et al.'s [18] model. ASLUM v3.1 simulate rows of street trees as circular shapes in the cross-sectional (2D) plane (Fig. 2a). Due to the relatively small size of tree trunks as compared to tree crowns and other urban facets, the impacts of trunks on radiation exchange are neglected [17–19]. For illustration, here we assume one row of trees to simplify the interactions between trees (see Section 3.3), while the proposed model can still simulate multiple rows of trees as in ASLUM v3.0 [24,25]. The size and location of trees within the street canyon are determined by three geometric parameters (Fig. 2a): the distance between the wall and the center of the tree crown ("wall–tree distance", d_T), the height of the tree crown center ("tree height", h_T), and the radius of the tree crown (r_T). For one row of trees herein, d_T is equal to half the canyon width (i.e., at the center of the street canyon) in a symmetric street canyon.

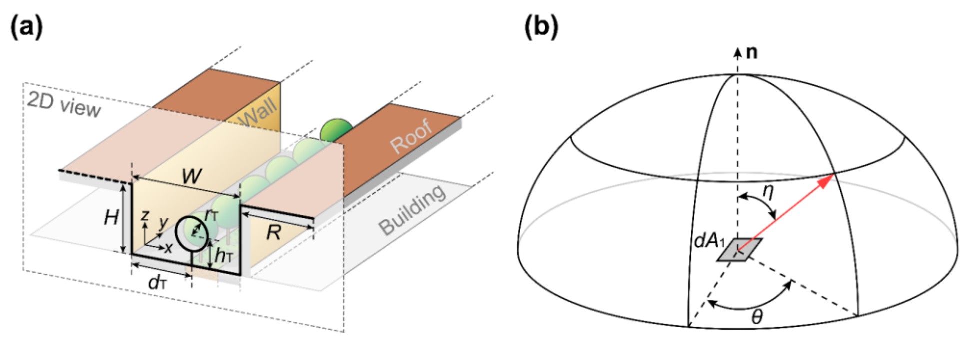

Figure 2. (a) Schematic structure of ASLUM v3.1 with one row of street trees and (b) the direction of an energy bundle leaving an elemental surface area dA_1 (red arrow) determined by its zenith angle η and azimuth angle θ. Note that in (a), H, W, and R are building height, road width, and roof width, respectively, d_T is the distance between the wall and the center of the tree

crown, h_T is the height of the tree crown center, and r_T is the radius of the tree crown. In (b), **n** is the normal vector to the surface area.

(Figure 2 is a 1.5-column fitting image)

3. Model description

3.1 Analytical solutions of radiative view factors

A radiative view factor F_{12} describes the geometric relation of two surfaces (A_1 and A_2) as the fraction of uniform diffuse radiation leaving a surface A_1 that directly reaches another surface A_2 [42]. In general, the direction of an energy bundle leaving an elemental surface area can be specified by the zenith angle η and azimuth angle θ in a spherical coordinate system centered on it (Fig. 2b). The differential view factor between two elemental surface areas (from dA_1 to dA_2) is calculated as

$$dF_{dA_1dA_2} = \frac{\cos\eta_1 \cos\eta_2}{\pi S^2} dA_2, \tag{1}$$

where η_1 (η_2) is the zenith angle between the energy bundle and the surface normal of dA_1 (dA_2), and S is the length of the bundle. Integrating Eq. (1) over both surfaces gives

$$F_{12} = \frac{1}{A_1} \int_{A_1} \int_{A_2} \frac{\cos\eta_1 \cos\eta_2}{\pi S^2} dA_2 dA_1 \ . \tag{2}$$

For street canyons without trees in ASLUM v1.x and v2.x (Fig. 1), the view factors can be analytically determined as [57]

$$F_{\mathrm{SG}} = F_{\mathrm{GS}} = \sqrt{1 + \left(\frac{H}{W}\right)^2} - \frac{H}{W}, \tag{3}$$

$$F_{\mathrm{WW}} = \sqrt{1 + \left(\frac{W}{H}\right)^2} - \frac{W}{H}, \tag{4}$$

$$F_{GW} = \frac{1}{2}\left(1 - F_{GS}\right), \quad (5)$$

$$F_{WG} = F_{WS} = \frac{1}{2}\left(1 - F_{WW}\right), \quad (6)$$

where the subscripts S, G, and W denote sky, ground, and wall, respectively, H is the building height, and W is the ground (road) width (see also Fig. 2a). The ratio H/W is called canyon aspect ratio.

For street canyons with one row of trees, the radiative view factor from trees (simplified as circles in the 2D view) to one wall can also be analytically solved [58],

$$F_{TW} = \frac{1}{\pi}\arctan\left(\frac{H}{2d_T}\right). \quad (7)$$

We can easily derive the view factor from wall to trees by applying the reciprocity relation (i.e., $A_1F_{12} = A_2F_{21}$),

$$F_{WT} = \frac{2r_T}{H}\arctan\left(\frac{H}{2d_T}\right). \quad (8)$$

3.2 Numerical solutions of radiative view factors with Monte Carlo ray tracing

The analytical solutions in Section 3.1 were developed based on simple geometry with opaque surfaces, and are not applicable to complex geometries such as multiple rows of trees (e.g., two rows as in [24,25]) or, in particular, trees with transmittance considered. As an alternative approach, the Monte Carlo method has been proposed to solve the radiation exchange in enclosures and view factors [17,42]. In Monte Carlo ray tracing, the amount of radiative energy can be numerically discretized into bundles (packets or rays) of energy. If equal energies are assigned to all energy bundles, the local energy flux can be computed by counting the number of bundles reaching a position of interest [42]. Similarly, the view factor F_{12} can be determined by the proportion of rays emitted from surface A_1 that are incident on surface A_2 (ratio of ray numbers).

Following the definition of bundle angles in Fig. 2b, the zenith angle η and azimuth angle θ for a diffuse–gray surface are randomized using two random numbers R_η and R_θ,

$$R_\eta = \sin^2 \eta , \tag{9}$$

$$R_\theta = \frac{\theta}{2\pi} . \tag{10}$$

It is straightforward that the direction of a ray can be transformed from its local spherical coordinate system to a local Cartesian coordinate system as,

$$\begin{bmatrix} \sin\eta\cos\theta \\ \sin\eta\sin\theta \\ \cos\eta \end{bmatrix} = \begin{bmatrix} \cos\theta & -\sin\theta & 0 \\ \sin\theta & \cos\theta & 0 \\ 0 & 0 & 1 \end{bmatrix} \begin{bmatrix} \sin\eta \\ 0 \\ \cos\eta \end{bmatrix} . \tag{11}$$

This direction vector in the local Cartesian coordinate system is then transformed to the global Cartesian coordinate system (Fig. 2a) via translation and rotation.

The emitting coordinates of rays from horizontal and vertical facets (ground, sky, and walls) are determined by random numbers R_x and R_z [17],

$$x_e = WR_x,\ z_e = 0 \text{ or } H, \text{ from ground or sky,} \tag{12}$$

$$x_e = 0 \text{ or } W,\ z_e = HR_z, \text{ from walls.} \tag{13}$$

The emitting coordinates of rays from the surface of tree crowns are given by a random number R_e,

$$x_e = d_T + r_T \sin(2\pi R_e), \tag{14}$$

$$z_e = h_T + r_T \cos(2\pi R_e). \tag{15}$$

Note that the above five random numbers (R_η, R_θ, R_x, R_z, and R_e) are random numbers between zero and one sampled from the standard uniform distribution. Usually these random numbers can be generated by the pseudorandom number generator in MATLAB [17,19], but the ray tracing methods using such random numbers have a slow convergence rate [59]. Instead, here we use the Latin hypercube sampling method to generate random numbers that spread more evenly across the sample space. The latter method is expected to speed up the convergence with smaller discrepancies from the analytical solutions (see Section 4.1).

Different from the implicit method proposed by Wang [17] in ASLUM v3.0, here we track the incident location of each ray by explicitly solving its intersections with all boundaries in Fig. 2a. For example, the intersection of the ray with a horizontal or vertical facet (if there is a single intersection) is $\mathbf{l}_e + \mathbf{l}d$. Here $\mathbf{l}_e$ is the emitting point, $\mathbf{l}$ is the direction vector of the ray, and d is solved by

$$d = \frac{(\mathbf{p}_0 - \mathbf{l}_e)\cdot\mathbf{n}}{\mathbf{l}\cdot\mathbf{n}}, \tag{16}$$

where $\mathbf{p}_0$ is a point on the facet, and $\mathbf{n}$ is a normal vector to the facet as in Fig. 2b. We then determine the actual incident point with the shortest distance from the emitting point.

We further consider the impact of canopy transmittance on the radiative view factors. For simplicity, here we assume that the tree foliage is randomly distributed (spatial homogeneity), the leaf inclination angles are spherically distributed, and the individual leaf size is much smaller than the crown size. These assumptions have been commonly used in previous studies (especially those on urban tree modeling) [18,20,60]. With these assumptions, the transmittance is equivalent to the canopy gap fraction [61,62]. In the proposed ray tracing model, the transmittance of tree crowns for both direct and diffuse radiation is a function of leaf area index (LAI) based on the Beer–Lambert law [60,63],

$$\tau = e^{-k\mathrm{LAI}}, \tag{17}$$

where k is an empirical light extinction coefficient. We assume $k = 0.61$ following measurements in a deciduous forest ecosystem [63]. It is noteworthy that although this coefficient was from photosynthetically active radiation measurements only, it is still within the ranges of extinction coefficients for broad-leaved forests [60]. Here we use this empirical function to represent the fraction of view unobstructed by canopy (similar to porous media; cf. transmittance of longwave radiation assumed to be zero in e.g., Konarska et al. [64]). The transmittance τ is then used as the probability of a ray propagating through the tree canopy once it reaches the tree crown surface.

3.3 Radiation exchange and turbulent heat fluxes in ASLUM v3.1

The direct shortwave radiation for trees is determined by reference angles. In ASLUM v3.1 with one row of trees, two reference angles are needed (Fig. 3a and b),

$$\tan\theta_{ref_1} = \frac{r_\mathrm{T}(H-h_\mathrm{T}) + d_\mathrm{T}\sqrt{d_\mathrm{T}^2 + (H-h_\mathrm{T})^2 - r_\mathrm{T}^2}}{(H-h_\mathrm{T})\sqrt{d_\mathrm{T}^2 + (H-h_\mathrm{T})^2 - r_\mathrm{T}^2} - r_\mathrm{T} d_\mathrm{T}}, \quad (18)$$

$$\tan\theta_{ref_2} = \frac{d_\mathrm{T}\sqrt{d_\mathrm{T}^2 + (H-h_\mathrm{T})^2 - r_\mathrm{T}^2} - r_\mathrm{T}(H-h_\mathrm{T})}{(H-h_\mathrm{T})\sqrt{d_\mathrm{T}^2 + (H-h_\mathrm{T})^2 - r_\mathrm{T}^2} + r_\mathrm{T} d_\mathrm{T}}. \quad (19)$$

The direct shortwave radiation incident on trees is determined as [18]

$$S_{D,\mathrm{T}} = \begin{cases} 0 & \text{if } \xi \ge \tan\theta_{ref_1} \\ S_D[r_\mathrm{T}\sqrt{1+\xi^2} + d_\mathrm{T} - (H-h_\mathrm{T})\xi]/(2\pi r_\mathrm{T}) & \text{if } \tan\theta_{ref_2} \le \xi \le \tan\theta_{ref_1} \\ S_D(2r_\mathrm{T}\sqrt{1+\xi^2})/(2\pi r_\mathrm{T}) & \text{if } \xi \le \tan\theta_{ref_2} \end{cases}, \quad (20)$$

where S_D is the direct solar radiation received by a horizontal surface, $\xi = \tan\theta_z \sin|\theta_n|$, θ_z is the solar zenith angle, and θ_n is the difference between the solar azimuth angle and canyon orientation [13,27]. Note that unlike in Ryu et al. [18], the transmittance is absent in the final equations of direct shortwave radiation for trees, as the equivalent crown surface area becomes $(1-\tau)2\pi r_T$ here.

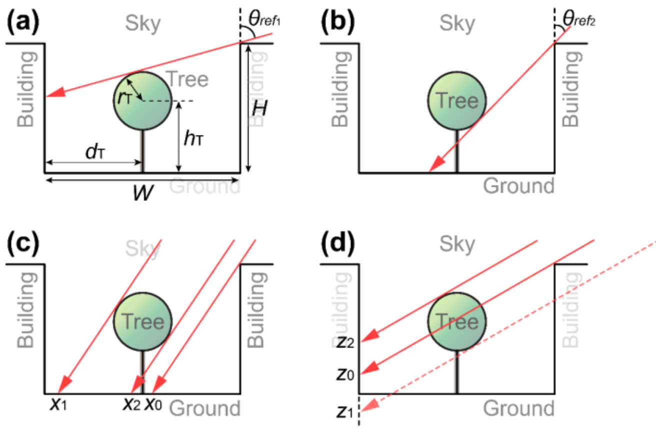

Figure 3. Determination of direct shortwave radiation in ASLUM v3.1 using (a) and (b) reference angles and (c) and (d) reference points.

(Figure 3 is a single column fitting image)

Six reference points are used to determine shadows cast by wall and trees, as shown in Fig. 3c and d. Points $(x_0, 0)$ and $(0, z_0)$ are the intersections of the ray passing the upper corner of one wall with the ground and the other wall, respectively [18],

$$x_0 = \max[W - H\xi, 0], \tag{21}$$

$$z_0 = \max[H - W/\xi, 0]. \tag{22}$$

The two reference points delimiting tree shadow from the sunlit ground are

$$x_1 = \max[d_T - h_T\xi - r_T\sqrt{1+\xi^2}, 0], \tag{23}$$

$$x_2 = \max[d_T - h_T\xi + r_T\sqrt{1+\xi^2}, 0], \tag{24}$$

and the two reference points delimiting tree shadow from the sunlit wall are

$$z_1 = \max[h_T - d_T\xi^{-1} - r_T\sqrt{1+\xi^{-2}}, 0], \tag{25}$$

$$z_2 = \max[h_T - d_T\xi^{-1} + r_T\sqrt{1+\xi^{-2}}, 0]. \tag{26}$$

Here $x_1 < x_2$ and $z_1 < z_2$. Then the shadow length on the ground from trees, if the shadow cast by the wall is not considered, is $\chi_T = x_2 - x_1$. Similarly, the shadow length on the wall due to trees is $\lambda_T = z_2 - z_1$.

Then the total shadow length on the ground due to wall and trees is

$$\chi_{\text{shadow}} = \begin{cases} W - x_0 + \chi_T & \text{if } x_2 \le x_0 \\ W + \chi_T - x_2 & \text{if } x_1 \le x_0 < x_2 \\ W - x_0 & \text{if } x_0 < x_1 \end{cases}, \tag{27}$$

and the shadow length on the ground due exclusively to trees is

$$\chi_{\text{trees}} = \begin{cases} \chi_T & \text{if } x_2 \le x_0 \\ \chi_T - (x_2 - x_0) & \text{if } x_1 \le x_0 < x_2 \\ 0 & \text{if } x_0 < x_1 \end{cases}. \tag{28}$$

The total shadow length on the wall due to wall and trees is

$$\lambda_{\text{shadow}} = \begin{cases} \max[z_0, z_2] & \text{if } z_1 \le z_0 \\ \lambda_T + z_0 & \text{if } z_0 < z_1 \end{cases}, \tag{29}$$

and the shadow length on the wall due exclusively to trees is

$$\lambda_{\text{trees}} = \begin{cases} 0 & \text{if } z_2 \le z_0 \\ z_2 - z_0 & \text{if } z_1 \le z_0 < z_2 \\ \lambda_T & \text{if } z_0 < z_1 \end{cases}. \tag{30}$$

The direct shortwave radiation incident on the ground is calculated as

$$S_{D,G} = S_D(W - \chi_{\text{shadow}} + \tau\chi_{\text{trees}}) / W, \tag{31}$$

and the direct shortwave radiation incident on walls is

$$S_{D,W} = S_D\xi(H - \lambda_{\text{shadow}} + \tau\lambda_{\text{trees}}) / (2H). \tag{32}$$

The term $\tau\lambda_{\text{trees}}$ and $\tau\chi_{\text{trees}}$ represent the sunflecks under trees at a particular solar angle. Note that different from Ryu et al. [18] and Meili et al. [19], one row of trees in the proposed model involves no interference between trees in the *x*-*z* plane (Fig. 2a), so that the redistribution of energy excess or deficit (due to the neglection of interference, as in previous studies) is unnecessary.

The net shortwave radiation for each facet (ground, walls, roof, and tree crowns) is the absorption of the direct and reflected shortwave radiation. We assume Lambertian surfaces as in Kusaka et al. [13]. The subfacet heterogeneity is also resolved following Wang et al. [27]. Here we only show equations related to tree crowns, and solutions for other facets are similar to those detailed in Wang et al. [27]. For trees, the net shortwave radiation is

$$S_{\mathrm{T}} = (1-\alpha_{\mathrm{T}})[S_{D,\mathrm{T}} + S_Q F_{\mathrm{TS}} + 2(S_{D,\mathrm{W}} + S_Q F_{\mathrm{WS}})\overline{\alpha_{\mathrm{W}}} F_{\mathrm{TW}} + (S_{D,\mathrm{G}} + S_Q F_{\mathrm{GS}})\overline{\alpha_{\mathrm{G}}} F_{\mathrm{TG}}], \quad (33)$$

where α_{T} is the albedo of trees, $\overline{\alpha_{\mathrm{W}}}$ and $\overline{\alpha_{\mathrm{G}}}$ are the equivalent albedos of walls and ground with subfacets, respectively, and S_Q is the diffuse solar radiation received by a horizontal surface.

The net longwave radiation absorbed by trees also considers both direct and reflected radiation,

$$L_{\mathrm{T},direct} = \varepsilon_{\mathrm{T}}(L^{\downarrow} F_{\mathrm{TS}} + 2\overline{\varepsilon_{\mathrm{W}}}\sigma\overline{T_{\mathrm{W}}}^4 F_{\mathrm{TW}} + \overline{\varepsilon_{\mathrm{G}}}\sigma\overline{T_{\mathrm{G}}}^4 F_{\mathrm{TG}} - \sigma T_{\mathrm{T}}^4), \quad (34)$$

$$\begin{aligned} L_{\mathrm{T},reflected} = \varepsilon_{\mathrm{T}}[&2F_{\mathrm{TW}}(1-\overline{\varepsilon_{\mathrm{W}}})(L^{\downarrow} F_{\mathrm{WS}} + \overline{\varepsilon_{\mathrm{W}}}\sigma\overline{T_{\mathrm{W}}}^4 F_{\mathrm{WW}} + \overline{\varepsilon_{\mathrm{G}}}\sigma\overline{T_{\mathrm{G}}}^4 F_{\mathrm{WG}} + \varepsilon_{\mathrm{T}}\sigma T_{\mathrm{T}}^4 F_{\mathrm{WT}}) \\ &+ F_{TG}(1-\overline{\varepsilon_{\mathrm{G}}})(L^{\downarrow} F_{\mathrm{GS}} + 2\overline{\varepsilon_{\mathrm{W}}}\sigma\overline{T_{\mathrm{W}}}^4 F_{\mathrm{GW}} + \varepsilon_{\mathrm{T}}\sigma T_{\mathrm{T}}^4 F_{\mathrm{GT}})] \end{aligned}, \quad (35)$$

where ε_{T} is the emissivity of trees, $\overline{\varepsilon_{\mathrm{W}}}$ and $\overline{\varepsilon_{\mathrm{G}}}$ are the equivalent emissivities of walls and ground with subfacets, respectively, σ is the Stefan–Boltzmann constant, T_{T} is the tree temperature, $\overline{T_{\mathrm{W}}}$ and $\overline{T_{\mathrm{G}}}$ are the equivalent temperatures of walls and ground, respectively, and $L^{\downarrow}$ is the downward longwave radiation.

The turbulent heat fluxes (sensible and latent heat fluxes) from walls, ground, and roof are determined via resistance networks (Fig. 1), as detailed in Wang et al. [27]. ASLUM v3.1 also considers water-holding capacity of engineered pavements, and calculates the latent heat flux from natural surfaces with reduction factor and stomatal resistance as in previous versions [27,50]. For trees, the transpiration per unit of leaf plan area for a single, hypostomatous leaf is given as [18,65]

$$E_{\mathrm{leaf}} = \frac{sR_{\mathrm{n}} + 0.93\rho c_{\mathrm{p}} D_{\mathrm{a}} / r_{\mathrm{a}}}{L_{\mathrm{v}}[s + 0.93\gamma(2 + r_{\mathrm{s}} / r_{\mathrm{a}})]}, \tag{36}$$

where s is the slope of the saturation vapor pressure curve at the ambient air temperature, ρ is the density of air, c_{p} is the specific heat capacity of air at a constant temperature, D_{a} is the vapor pressure deficit of air, r_{a} and r_{s} are boundary layer resistance and stomatal resistance of the leaf, respectively, L_{v} is the latent heat of vaporization, and γ is the psychrometric constant. Note that the leaf boundary layer resistance follows the empirical relation in Green [65]. The net radiation of the leaf, R_{n}, is the sum of net shortwave radiation (S_{leaf}) and net longwave radiation (L_{leaf}),

$$S_{\mathrm{leaf}} = \frac{S_{\mathrm{T}} 2\pi r_{\mathrm{T}} (1-\tau)}{2r_{\mathrm{T}}\mathrm{LAI}}, \tag{37}$$

$$L_{\mathrm{leaf}} = \frac{L_{\mathrm{T}} 2\pi r_{\mathrm{T}} (1-\tau)}{2r_{\mathrm{T}}\mathrm{LAI}}, \tag{38}$$

where $L_{\mathrm{T}} = L_{\mathrm{T},\mathit{direct}} + L_{\mathrm{T},\mathit{reflected}}$, and $2r_{\mathrm{T}}\mathrm{LAI}$ is the total leaf plan area. The latent heat flux per unit leaf plan area is then $LE_{\mathrm{leaf}} = L_{\mathrm{v}}E_{\mathrm{leaf}}$.

The sensible heat flux per unit leaf plan area is given as

$$H_{\mathrm{leaf}} = \frac{\rho c_{\mathrm{p}} (T_{\mathrm{T}} - T_{\mathrm{can}})}{\mathrm{RES}_{\mathrm{leaf}}}, \tag{39}$$

where T_{can} is the street canyon air temperature, and the aerodynamic resistance $\mathrm{RES}_{\mathrm{leaf}} = 1.27r_{\mathrm{a}}$ [18,66].

ASLUM v3.1 simulates the root water uptake by vegetation as a sink term in the Richards equation using an empirical model developed by Jarvis [67]. This method takes into account the effects of vertical distributions of roots and soil water content, and we assume the total root water uptake to be equal to the total transpiration. More details of root water uptake calculation can be found in Ryu et al. [18]. Note a tree fraction parameter (e.g., Eq. (21) in Ryu et al. [18]) is not needed here, as ASLUM assumes homogeneity in the along-canyon axis (2D street canyon).

The canyon air temperature can be diagnostically solved as

$$T_{\mathrm{can}} = \frac{\frac{2H}{W}\frac{\overline{T_{\mathrm{W}}}}{\mathrm{RES_W}} + \frac{\overline{T_{\mathrm{G}}}}{\mathrm{RES_G}} + \frac{2r_{\mathrm{T}}\mathrm{LAI}}{W}\frac{T_{\mathrm{T}}}{\mathrm{RES_{leaf}}} + \frac{T_{\mathrm{a}}}{\mathrm{RES_{can}}}}{\frac{2H}{W}\frac{1}{\mathrm{RES_W}} + \frac{1}{\mathrm{RES_G}} + \frac{2r_{\mathrm{T}}\mathrm{LAI}}{W}\frac{1}{\mathrm{RES_{leaf}}} + \frac{1}{\mathrm{RES_{can}}}}, \tag{40}$$

where $\mathrm{RES_W}$, $\mathrm{RES_G}$, and $\mathrm{RES_{can}}$ are aerodynamic resistances of wall, ground, and street canyon, and T_{a} is the air temperature at the reference height. This approach has been used in Masson [12] and Wang et al. [27], although not for urban trees. Similarly, the canyon air specific humidity can be diagnostically solved as

$$q_{\mathrm{can}} = \frac{\frac{\rho L_{\mathrm{v}}\overline{q_{\mathrm{G}}}}{\mathrm{RES_G}} + \frac{\rho L_{\mathrm{v}} q_{\mathrm{a}}}{\mathrm{RES_{can}}} + \frac{2r_{\mathrm{T}}\mathrm{LAI}}{W} LE_{\mathrm{leaf}}}{\frac{\rho L_{\mathrm{v}}}{\mathrm{RES_{can}}} + \frac{\rho L_{\mathrm{v}}}{\mathrm{RES_G}}}, \tag{41}$$

where $\overline{q_{\mathrm{G}}}$ is the equivalent specific humidity of ground, and q_{a} is the specific humidity at the reference height.

4. Model evaluation

4.1 Monte Carlo simulations and analytical solutions of radiative view factors in street canyons without trees

We compare the estimated view factors using the Monte Carlo ray tracing method against analytical solutions based on Eqs. (3)–(6) in street canyons without trees (ASLUM v1.x and v2.x). Results of F_{SG} and F_{WS} using different random number generators and sample sizes (for each urban facet) are shown as the deviations from analytical solutions ("errors") in Fig. 4. For both (pseudo)random number generators, the accuracy of Monte Carlo ray tracing increases with the sample size *N*. The estimated results with relatively higher errors usually occur within the *H*/*W* range of 0.1–10. With a sample size of 50000, the ray tracing methods using both random number generators yield results with high accuracies: the values of mean absolute error (MAE) are below 0.001. On the other hand, the ray tracing algorithm using the Latin hypercube sampling method converges much faster than that using the default pseudorandom number generator. For example, when the sample size is 100 (not shown here), the MAE of the estimated F_{SG} with the Latin hypercube sampling method is 0.008, much lower than that with the default generator (0.02). In the subsequent simulations, we use the Latin hypercube sampling method with a sample size of 10000 in the Monte Carlo ray tracing algorithm. This ensures both high accuracy (MAE < 0.001) and computational efficiency when estimating view factors.

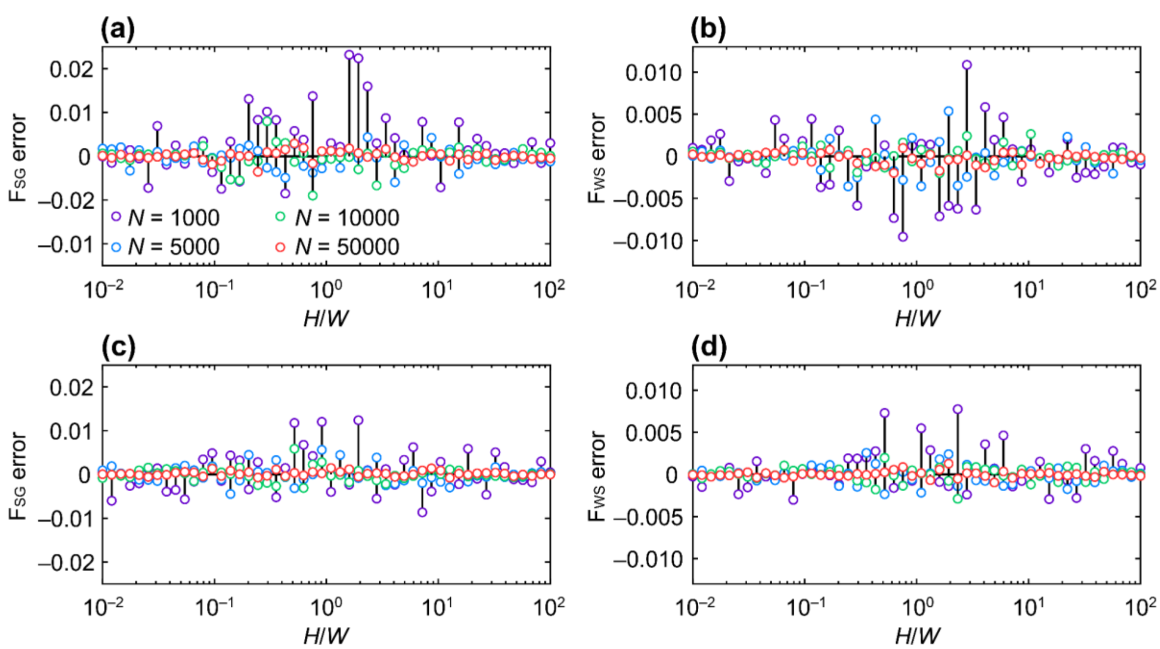

Figure 4. Numerical errors of view factors F_{SG} and F_{WS} with varying canyon aspect ratio H/W estimated using the Monte Carlo ray tracing method as compared to analytical solutions in street canyons without trees. In Monte Carlo simulations, (a) and (b) use the default pseudorandom number generator in MATLAB, whereas (c) and (d) use the Latin hypercube sampling method. Note that N is the sample size for each urban facet.

(Figure 4 is a 2-column fitting image)

Figure 5 shows the comparison between the estimated view factors using the Monte Carlo ray tracing method and their analytical solutions as functions of the canyon aspect ratio. The proposed ray tracing method reproduces analytical solutions with nearly negligible discrepancies. In particular, radiative view factors drastically change when the canyon aspect ratio is in the range of 0.1–10. This partially explains the relatively high errors within the same range observed in Fig. 4. This range is also similar to that for real cities (0.05–5 in Harman et al. [57]; 0.2–10 in Wang [17]), suggesting that it is critical to accurately estimate view factors in realistic urban street canyons.

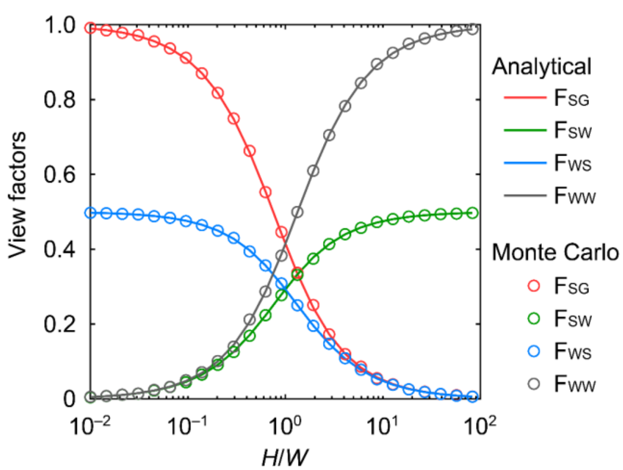

Figure 5. View factors F_{SG}, F_{SW}, F_{WS}, and F_{WW} with varying canyon aspect ratio H/W estimated using the Monte Carlo ray tracing method and their analytical solutions in street canyons without trees. The sample size $N = 10000$.

(Figure 5 is a single column fitting image)

4.2 Monte Carlo simulations and analytical solutions of radiative view factors in street canyons with trees

We evaluate the estimated view factors between one wall and trees using the Monte Carlo ray tracing method against their analytical solutions using Eqs. (7) and (8) in street canyons with one row of trees (ASLUM v3.x). Results are shown in Fig. 6 as functions of canyon aspect ratio, normalized tree crown radius (r_T/W), and normalized wall–tree distance (d_T/W). Across the entire spectrum of d_T/W, both radiative view factors estimated by Monte Carlo simulations are in good agreement with analytical solutions. In general, both F_{TW} and F_{WT} increase as the wall–tree distance decreases, because the hemispherical envelope of an element on the wall tends to be more occupied by trees when d_T is smaller. Deeper canyons with higher aspect ratio reduce the view factor F_{WT} as the dimension of wall increases (Fig. 6b); meanwhile, greater F_{TW} values are observed based on the reciprocity relation (Fig. 6a). F_{TW} is not affected by varying tree crown radius (see also Eq. (7)). As an example, Figure 6c shows F_{TW} for $r_T/W = 0.175$. In contrast, the view factor F_{WT} estimated by Monte Carlo simulations linearly declines with tree crown radius (Fig. 6d), consistent with the analytical solution based on Eq. (8). Figure 6 suggests that the proposed Monte Carlo ray tracing method can accurately predict tree-related view factors for varying geometries of both street canyons and trees.

We also compare the proposed method with the previous algorithm in ASLUM v3.0 [17]. Here we assume that $H/W = 0.3$, $r_T = 0.09W$, $h_T = 0.5H$, and $d_T = 0.5W$ for demonstration. Results are summarized in Table 2. Considering that the proposed ray tracing method is robust and accurate (Figs. 4–6), here we treat its results as the "ground truth" in comparison. Although both methods can accurately predict view factors in street canyons without trees [17], clear discrepancies are found for street canyons with trees. In particular, with a simplified and implicit representation of tree crowns, Wang's [17] method underestimates F_{TW} by over 51% when compared to the proposed method. This comparison, as an example, highlights the improved performance of the proposed method when compared to its previous version [17].

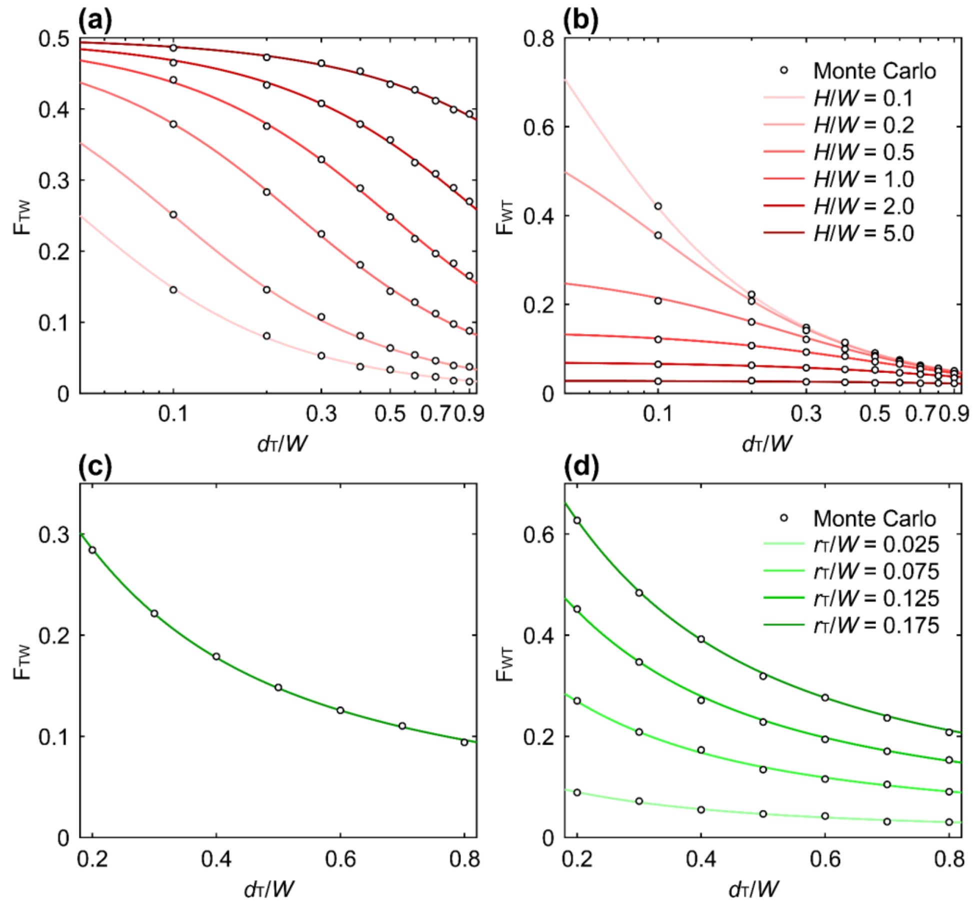

Figure 6. View factors F_{TW} and F_{WT} estimated using the Monte Carlo ray tracing method and their analytical solutions in street canyons with trees as functions of (a) and (b) canyon aspect ratio H/W and normalized wall–tree distance d_T/W ($r_T = 0.045W$), and (c) and (d) normalized tree crown radius r_T/W and d_T/W ($H = 0.5W$). The tree height h_T is $0.5H$.

(Figure 6 is a 1.5-column fitting image)

Table 2. Comparison of view factors estimated using two Monte Carlo ray tracing methods.

	$F_{SG} = F_{GS}$	$F_{SW} = F_{GW}$	$F_{ST} = F_{GT}$	$F_{WS} = F_{WG}$	F_{WW}	F_{WT}	F_{TS}	F_{TG}	F_{TW}
Wang [17]	0.525	0.043	0.242	0.337	0.027	0.203	0.477	0.477	0.141
The proposed method	0.531	0.120	0.229	0.399	0.024	0.177	0.410	0.404	0.093
Error	–0.006	–0.077	0.014	–0.062	0.004	0.026	0.067	0.073	0.048

4.3 Sensitivity of radiative view factors to street canyon and tree geometry

In this section, we thoroughly evaluate the sensitivity of radiative view factors to the geometry of street canyon and trees. Note that $d_T = 0.5W$ follows the setting in ASLUM v3.1 (Section 2). Figure 7 shows the radiative view factors as functions of canyon aspect ratio and normalized tree crown radius. Here we set $W = 20$ m and $h_T = 4$ m, and calculate view factors with changing building height (8–40 m) and tree crown radius (0–3.8 m). When $r_T = 0$, the estimated view factors are identical to those in street canyons without trees, and the results of F_{TS} for r_T/W is not shown in Figs. 7 (same for Fig. 8). Among the eight view factors in Fig. 7, F_{SW}, F_{WS}, F_{WW}, and F_{TS} are relatively more sensitive to canyon aspect ratio than to tree crown radius. In contrast, F_{GT} is more sensitive to tree crown radius. Other view factors (F_{SG}, F_{ST}, and F_{WT}) exhibit high sensitivity in shallow street canyons ($H/W < \sim 1.2$). This is because the size of the tree (especially the largest one) is relatively comparable to that of walls in shallow canyons, and the radiation exchange between sky and ground can be largely intercepted by trees. However, the impacts of trees diminish as street canyons deepen. Due to similar reason, a local minimum of F_{WS} is observed with the shallowest street canyon and the largest tree crown radius in Fig. 7. With a constant canyon aspect ratio, view factors F_{ST}, F_{GT}, and F_{WT} linearly increase with tree crown radius, while F_{TS} remains intact (analogous to F_{TW} and F_{WT} in Fig. 6). Although the patterns of these view factors are in general consistent with those in Wang et al. [25], some minor discrepancies still exist, primarily because this previous study uses two rows of trees (cf. one row herein).

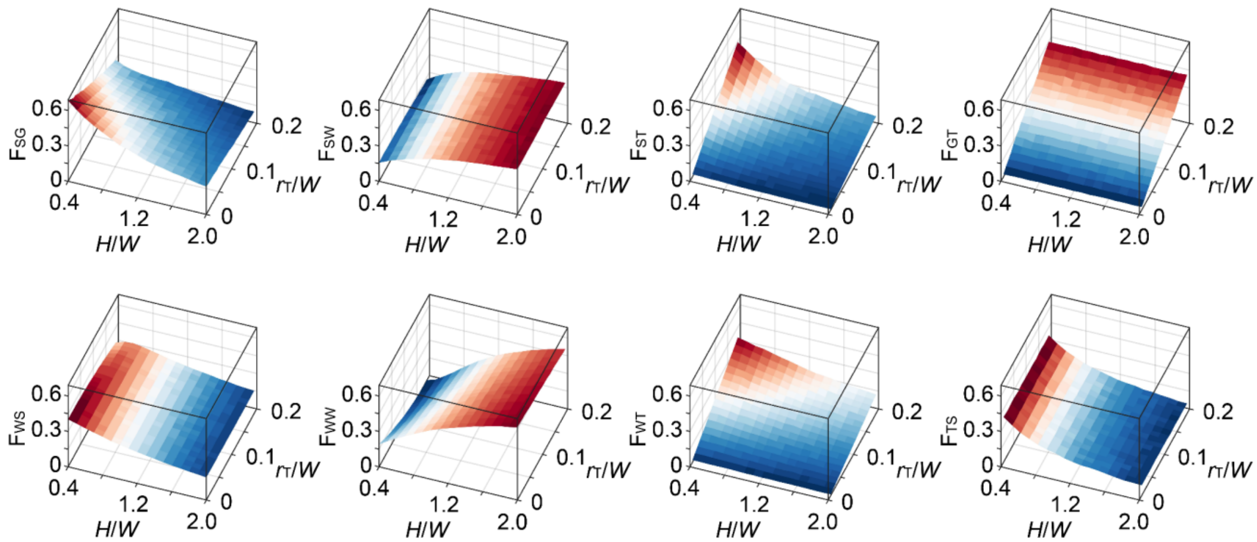

Figure 7. Sensitivity of radiative view factors to varying canyon aspect ratio (*H*/*W*) and normalized tree crown radius (r_T/W) in ASLUM v3.1. The wall–tree distance h_T equals 0.5*W*. Results are color coded such that red is for high values and blue is for low values.

(Figure 7 is a 2-column fitting image)

Figure 8 shows the radiative view factors as functions of normalized tree height and normalized tree crown radius. Here we set $W = 20$ m and $H = 20$ m, and calculate view factors with changing tree height (4–16 m) and tree crown radius (0–3.8 m). A canyon aspect ratio of 1.0 retains sufficiently nonlinear sensitivity of some view factors (F_{SG}, F_{ST}, and F_{WT}) to the normalized tree crown radius. As observed in Wang et al. [25], view factors between basic facets of the street canyon enclosure, i.e., F_{SG}, F_{SW}, F_{WS}, and F_{WW}, are relatively insensitive to tree height. F_{SW} and F_{WS} are also nearly intact with varying tree crown radius when tree crowns are close to the ground ($h_T/W <$ ~0.5), but slightly decrease when tree crowns become bigger and higher. View factors between two parallel facets (F_{SG} and F_{WW}) gradually drop as the tree crown size increases. Analogous to the view factor from one wall to trees with changing wall–tree distance (see Section 4.2), the view factors from ground/sky to trees nonlinearly change with tree height but linearly increases with tree radius (see Eq. (8)). Similarly, with constant tree height and wall–tree distance, the relationship between F_{WT} and tree crown size remains linear, which is in line with analytical solutions in Section 3.1. The view factor from trees to sky (F_{TS}) is independent of tree crown radius with a given tree height. It is noteworthy that the nonlinearity of view factors with varying geometry is not unusual (in fact is fairly common). This indicates that the generalized linear relationships between view factors and geometric parameters (e.g., H, r_T, and h_T) in Ryu et al. [18] are only applicable within certain ranges of geometry, and therefore need be used with caution.

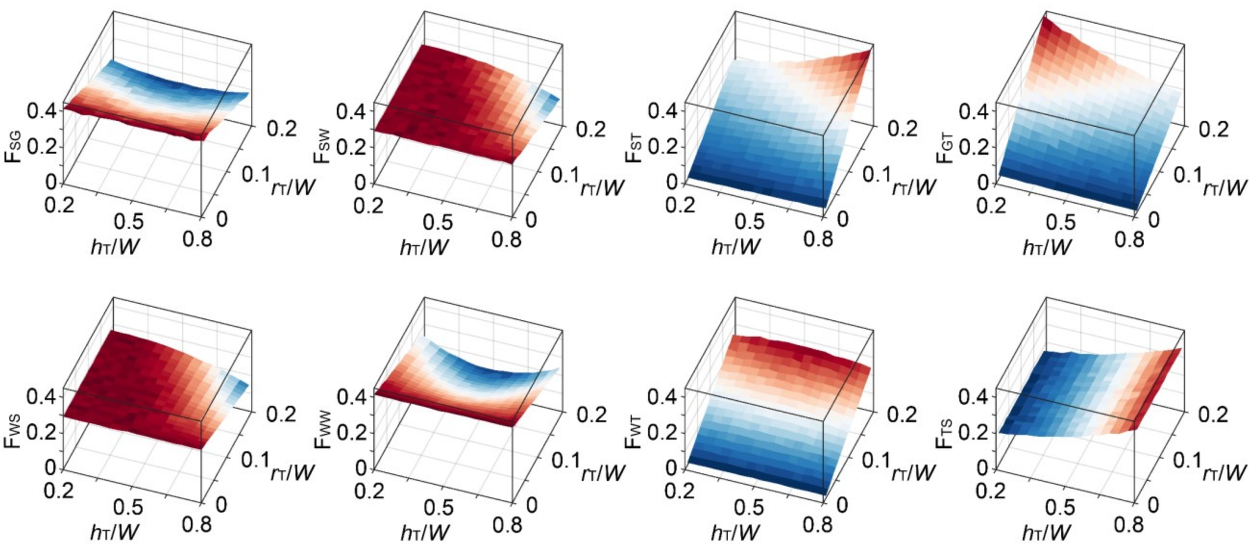

Figure 8. Same as Fig. 7 but for sensitivity to varying normalized tree height (h_T/W) and normalized tree crown radius (r_T/W).

(Figure 8 is a 2-column fitting image)

4.4 Sensitivity of radiative view factors to canopy transmittance

We further investigate the impacts of canopy transmittance on view factors. A set of geometric parameters is prescribed: $W = 20$ m, $h_T = 4$ m, $d_T = 10$ m ($0.5W$), $r_T = 3$ m, and changing H (8–40 m). Rather than using Eq. (17) with an empirical light extinction coefficient, here we manually set transmittance to range from 0.05 (very dense tree canopy) to 0.95 (very sparse tree canopy, e.g., induced by defoliation during cold seasons). Results of eight view factors are summarized in Fig. 9. In general, all view factors are nonlinearly dependent on the building height (or aspect ratio) except for F_{GT}, which is independent of varying H. This is in line with those shown in Fig. 7. For view factors between parallel canyon facets, F_{SG} and F_{WW} drastically increase with transmittance when the size of tree crown is comparable to the building height (shallow canyons). For example, F_{SG} increases by 0.283 when τ rises from 0.05 to 0.95. Similar but relatively mild increase with transmittance is observed for F_{SW} and F_{WS}. However, these distinct changes only occur in shallow street canyons, and the dependence of F_{SG}, F_{SW}, F_{WS}, and F_{WW} on transmittance rapidly diminishes as canyons become deeper. Among the four tree-related view factors, F_{TS} is the only one independent of transmittance, as the proportion of hemispherical envelope of tree crowns occupied by sky does not depend on the equivalent crown surface area (see also Eq. (20)). F_{ST}, F_{GT}, and F_{WT} gradually decrease in shallow street canyons as tree canopy becomes sparser. All eight view factors become closer to their no-tree counterparts (Section 4.3) when the transmittance drops toward zero. The considerable impact of τ on view factors, especially those related to trees, highlights that canopy transmittance plays an important role in the radiation exchange among urban facets. This also suggests that the seasonal variation of foliage should be considered in long-term simulations with street trees [19,25].

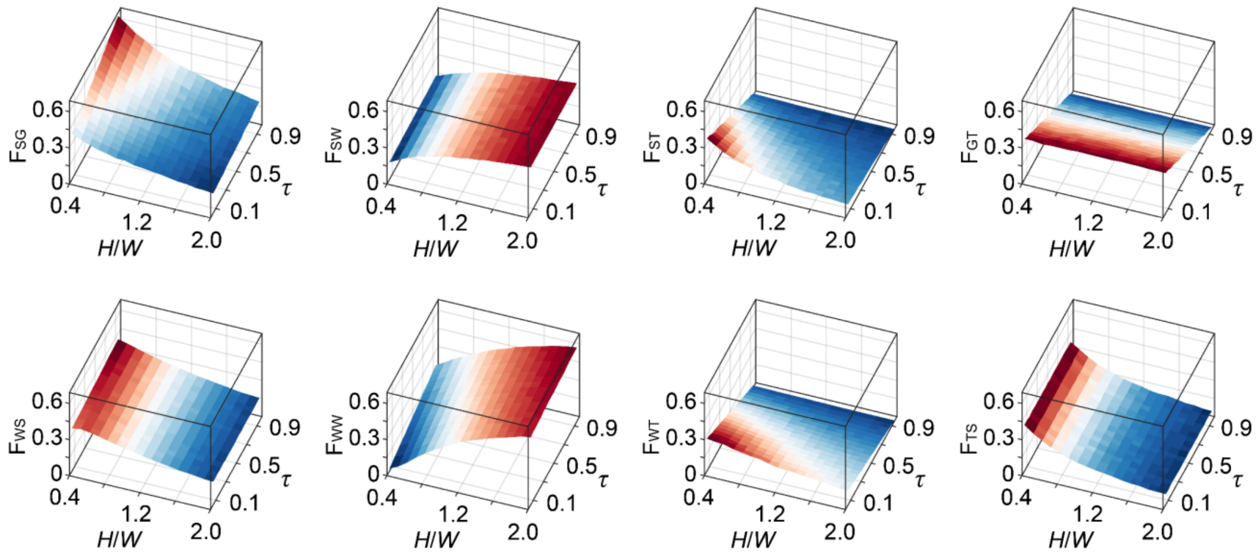

Figure 9. Same as Fig. 7 but for sensitivity to varying canyon aspect ratio (*H*/*W*) and canopy transmittance (τ).

(Figure 9 is a 2-column fitting image)

4.5 Evaluation of simulations against field observations

In this section, we evaluate the performance of the new ASLUM v3.1 and its previous version (ASLUM v2.0, basic v2.x) using field measurements from the Basel UrBan Boundary Layer Experiment (BUBBLE) campaign in Basel, Switzerland [68]. Specifically, we use observations from the urban Basel-Sperrstrasse site (47.57° N, 7.60° E) with the period of observations from June 10 to July 9, 2002 (30 days). A one-day spin-up period (June 9, 2020) is used. Details of the site and instruments employed during the experiment can be found in Rotach et al. [68]. The input parameters used in simulations with different versions of ASLUM are primarily from two previous studies [18,69] (Table 3). Note that Ryu et al. [18] use two rows of street trees (tree crown radius is 1.5 m) with a tree fraction of 0.8. In ASLUM v3.1 with only one row of trees, the equivalent tree crown radius, after taking into account transmittance (LAI = 4), is 3.4 m. Besides ASLUM v2.0 and v3.1, we also test a simplified version of ASLUM v3.1, in which the transmittance is neglected. Figure 10 shows the diurnal variations in observed and simulated street canyon air temperature, urban net radiation, urban sensible heat flux, and urban latent heat flux averaged over 30 days. To analyze the model performance, we calculate the coefficient of determination (R^2), root-mean-square error (RMSE), and mean bias error (MBE) following an international model comparison project [39,40]. The statistics are summarized in Table 4.

Table 3. Model parameters in simulations in Section 4.4.

Variables	Value	Versions
Street canyon and tree geometries		
Building height (m)	14.6	v2.0 and v3.1
Road (ground) width (m)	18.2	v2.0 and v3.1
Roof width (m)	21.4	v2.0 and v3.1
Reference height of atmospheric measurements (m)	31.7	v2.0 and v3.1
Thickness of roof (m)	0.3	v2.0 and v3.1
Thickness of wall (m)	0.3	v2.0 and v3.1
Distance between tree crown center and wall (m)	9.1	v3.1
Height of tree crown center (m)	7.3	v3.1
Tree crown radius (m)	3.4	v3.1
Leaf area index	4	v3.1
Fraction of subfacets on ground (asphalt, grass)	0.65, 0.35	v2.0 and v3.1
Roughness length		
Roughness length for momentum for canyon (m)	1.46	v2.0 and v3.1
Roughness length for momentum for roof (m)	0.15	v2.0 and v3.1
Roughness length for heat for canyon (m)	0.146	v2.0 and v3.1
Roughness length for heat for roof (m)	0.015	v2.0 and v3.1
Thermal properties		
Ground surface albedo (asphalt, grass)	0.10, 0.20	v2.0 and v3.1
Roof surface albedo	0.15	v2.0 and v3.1
Wall surface albedo	0.25	v2.0 and v3.1
Leaf surface albedo	0.20	v3.1
Ground surface emissivity (asphalt, grass)	0.95, 0.93	v2.0 and v3.1
Roof surface emissivity	0.95	v2.0 and v3.1
Wall surface emissivity	0.95	v2.0 and v3.1
Leaf surface emissivity	0.95	v3.1
Thermal conductivity of ground (W m^{-1} K^{-1}) (asphalt, grass)	1.2, 2.0	v2.0 and v3.1
Thermal conductivity of roof (W m^{-1} K^{-1})	0.94	v2.0 and v3.1
Thermal conductivity of wall (W m^{-1} K^{-1})	0.94	v2.0 and v3.1
Volumetric heat capacity of ground (MJ K^{-1} m^{-3}) (asphalt, grass)	1.8, 1.3	v2.0 and v3.1
Volumetric heat capacity of roof (MJ K^{-1} m^{-3})	1.4	v2.0 and v3.1
Volumetric heat capacity of wall (MJ K^{-1} m^{-3})	1.4	v2.0 and v3.1

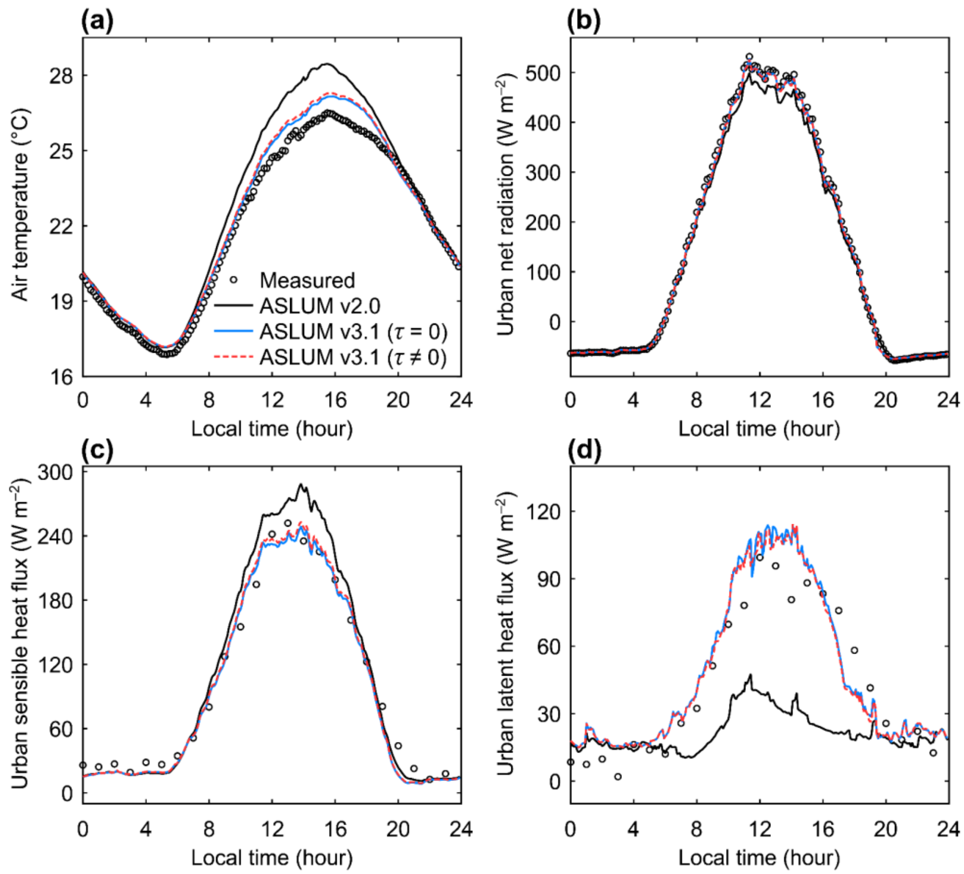

Figure 10. Simulated (a) street canyon air temperature, (b) urban net radiation, (c) urban sensible heat flux, and (d) urban latent heat flux using ASLUM v2.0 (without trees), v3.1 with $\tau = 0$, and v3.1 with $\tau \neq 0$ evaluated against measurements.

(Figure 10 is a 1.5-column fitting image)

On average, ASLUM v2.0 slightly overestimates the canyon air temperature (MBE = 0.86 °C) and the urban sensible heat flux (MBE = 5.19 W m^{-2}) while underestimates the urban net radiation (MBE = –11.38 W m^{-2}). However, the discrepancy in the simulated latent heat fluxes is relatively large (MBE = –20.62 W m^{-2}), primarily due to the omission of evapotranspiration from urban trees. The differences between simulations and observations of turbulent heat fluxes are even greater during the day (RMSE = ~47 W m^{-2}) than over the diurnal cycle (Fig. 10c and d) as the daytime surface energy balance is dominated by solar radiation.

Nevertheless, the performance of ASLUM v2.0 is in general consistent with and even better than the median performance of 32 urban land surface models in Grimmond et al. [39].

Table 4. Summary of performance statistics using different versions of ASLUM. Note that units are for RMSE and MBE, and the number of data points n = 8641 for each variable.

	R^2	RMSE	MBE
ASLUM v2.0 (without trees)			
Street canyon air temperature (°C)	0.98	1.25	0.86
Urban net radiation (W m^{-2})	1.00	19.01	–11.38
Urban sensible heat flux (W m^{-2})	0.87	40.73	5.19
Urban latent heat flux (W m^{-2})	0.24	40.34	–20.62
ASLUM v3.1 (with trees and τ = 0)			
Street canyon air temperature (°C)	0.99	0.63	0.34
Urban net radiation (W m^{-2})	1.00	7.95	–2.56
Urban sensible heat flux (W m^{-2})	0.86	36.83	–4.80
Urban latent heat flux (W m^{-2})	0.56	30.69	1.00
ASLUM v3.1 (with trees and τ = 0.087)			
Street canyon air temperature (°C)	0.99	0.69	0.40
Urban net radiation (W m^{-2})	1.00	8.36	–3.13
Urban sensible heat flux (W m^{-2})	0.87	36.85	–3.27
Urban latent heat flux (W m^{-2})	0.56	30.28	0.23

After including trees into ASLUM v3.1, clear improvement is observed in all three statistics of all four model outputs (Fig. 10 and Table 4). The most significant improvement is in latent heat flux (Fig. 10d), of which the RMSE decreases from 40.34 W m^{-2} to 30.28 W m^{-2}. The considerable underestimate of latent heat flux in ASLUM v2.0 is largely mitigated by the inclusion of trees: the MBE in latent heat flux in ASLUM v3.1 is 0.23 W m^{-2}. As a result, the systematic overestimate in sensible heat flux predicted by ASLUM v2.0 is also reduced via the changes in energy partitioning, especially during the daytime (Fig. 10c). Despite the minor overestimation, the predicted daytime air temperature is lower than that in ASLUM v2.0, showing the cooling effect of urban trees from shading and transpiration. The difference in the performance of ASLUM v2.0 and v3.1 highlights that the vegetation modeling plays an essential role in the simulation of urban surface energy flux exchanges [39]. It is noteworthy that the performance of ASLUM v3.1 is relatively better than that of Ryu et al.'s [18] model, which can be attributable to the more accurate ray tracing algorithm, the iteratively determined canyon air temperature and humidity, and the absence of artificial energy deficit/excess redistribution for tree–tree interactions in the ASLUM v3.1.

On the other hand, the impact of transmittance on the performance of ASLUM v3.1 with the input parameters in Table 3 is relatively weak, owing to the small transmittance of the dense tree canopy ($\tau = 0.087$) during summer. The statistics of the simulations using two versions of ASLUM v3.1 are quite close. Nevertheless, discrepancies in the simulated latent and sensible heat fluxes are still recognized. In particular, assuming the tree crowns to be opaque ($\tau = 0$) results in slightly overestimated urban latent heat flux (see Eq. (37) and (38)). For example, including transmittance can reduce the MBE of daytime urban latent heat flux from 2.37 W m^{-2} to 1.19 W m^{-2}. Such difference/improvement can be much greater when the transmittance of tree crowns is higher (Section 5.1).

5. Model applications and discussion

5.1 Radiation exchange and turbulent heat fluxes influenced by leaf area index

In this section, we evaluate the impacts of varying leaf area index and the associated transmittance on urban radiation exchange and turbulent heat fluxes. The input parameters are identical to those in Table 3 except for the LAI of trees (0–6 herein). We use ASLUM v2.0 for the case with LAI = 0 (without trees; reference case) and ASLUM v3.1 for the other five cases (LAI = 1–6). The simulated radiation budgets for different facets are shown in Fig. 11, and the simulated air temperature, net radiation, and turbulent heat fluxes are shown in Fig. 12. Note that tree net radiation is converted to leaf net radiation using Eqs. (37) and (38).

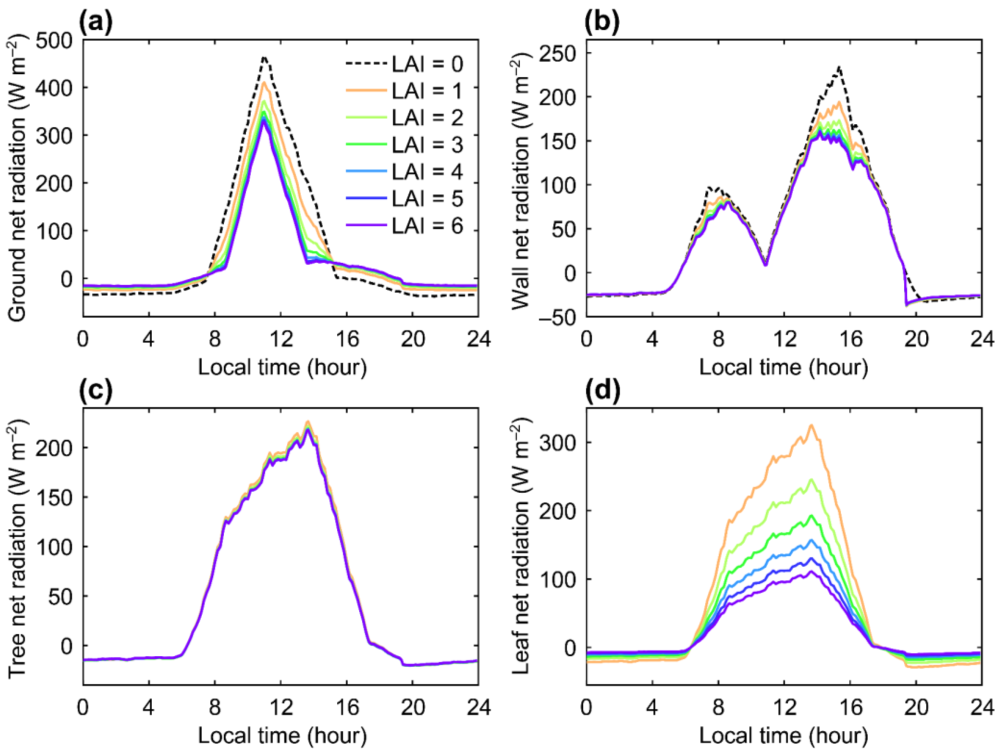

Figure 11. Simulated net radiations of (a) ground, (b) wall, (c) tree, and (d) leaf with varying leaf area index of trees.

(Figure 11 is a 1.5-column fitting image)

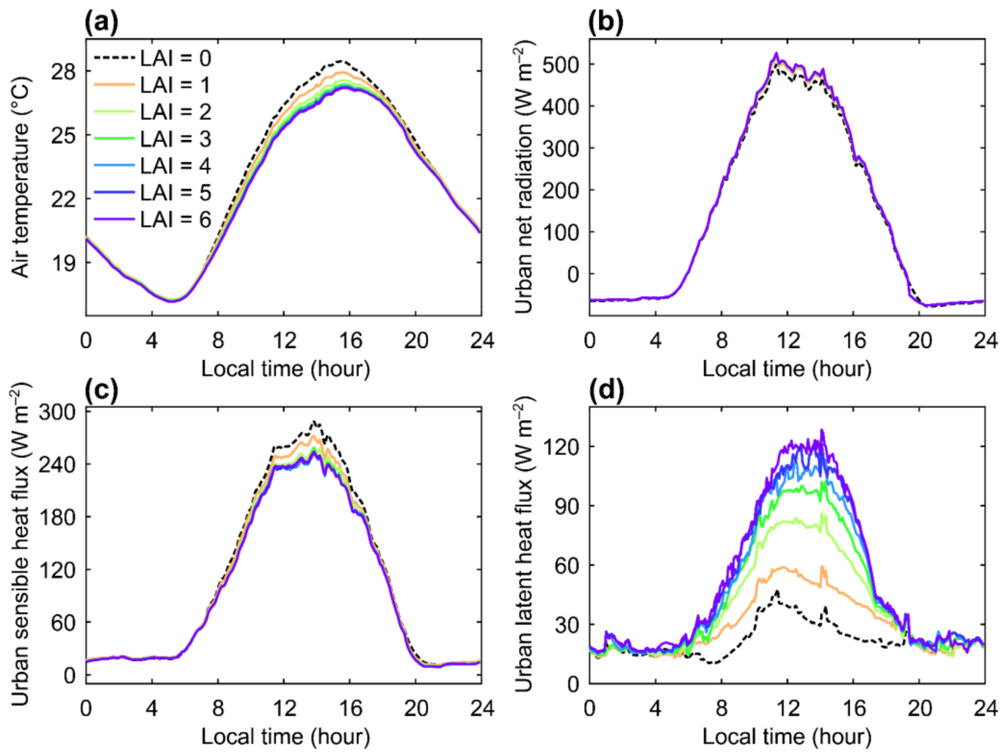

Figure 12. Simulated (a) street canyon air temperature, (b) urban net radiation, (c) urban sensible heat flux, and (d) urban latent heat flux with varying leaf area index of trees.

(Figure 12 is a 1.5-column fitting image)

As LAI of trees increases, the ground net radiation in general decreases during the daytime except for a few hours after sunrise and before sunset (Fig. 11a), primarily due to the strong shading effect of tree canopy [8,70]. Compared to the reference case (LAI = 0), urban trees with LAI = 6 reduce the average daytime ground net radiation by 42.58 W m^{-2} and the peak value by 139.31 W m^{-2} (maximum reduction is 172.69 W m^{-2}). However, increasing ground net radiation with LAI is observed at night, resulting from the radiative trapping effect of trees: the upward longwave radiation emitted from ground is partially blocked by tree canopy [25,41]. The average nighttime ground surface temperature in the case with LAI = 6 is even slightly warmer than in the reference case (0.4 °C higher). Similar reductions of daytime net radiation are also found for walls (Fig. 11b). On average, the daytime wall net radiation decreases by 17.71 W m^{-2}

as LAI increases from 0 to 6. The radiative trapping effect of trees on nighttime wall net radiation is relatively weaker than its ground counterpart. Note that the abrupt changes and the peaks of net radiation in Fig. 11 are determined by the shadow cast by walls and/or trees. The impact of varying LAI on the net radiation of trees is very marginal (Fig. 11c), as the determinant of this variable (direct shortwave radiation) is independent of transmittance (see Eq. (20)). But the difference in tree net radiation influenced by LAI and transmittance becomes much clearer when averaged over the leaf plan area (see Eqs. (37) and (38)). The mean daytime net radiation of leaf with LAI = 6 ($\tau = 0.026$) decreases by 83.71 W m^{-2} when compared to the case with LAI = 1 ($\tau = 0.543$) (the reduction in peak value is 213.87 W m^{-2}). The increasing LAI and diminishing transmittance jointly contribute to the observed changes in Fig. 11d. Note that the change in the impact of LAI gradually attenuates as it increases [18], resulting from the exponential nature of the LAI–τ relationship in Eq. (17).

The presence of street trees effectively lowers the daytime canyon air temperature. Compared to the reference case, the case with the densest tree canopy (LAI = 6) reduced the maximum daytime air temperature by ~1.3 °C (Fig. 12a). Owing to the reduced net radiation and surface temperature of canyon facets (ground and walls), the peak urban sensible heat flux of the same case is 34.91 W m^{-2} lower than in the case without trees (Fig. 12c), and the peak daytime ground and wall temperatures are reduced by 4.69 °C and 3.81 °C, respectively. Meanwhile, the average urban latent heat flux is enhanced by 43.75 W m^{-2} (maximum increase is 92.79 W m^{-2}; Fig. 12d). The reductions in air temperature and sensible heat flux, as well as the increases in latent heat flux, are nonlinearly dependent on LAI. In contrast, the changes in urban net radiation are relatively marginal (Fig. 12b). These changes clearly suggest that the synergistic interplay of radiative shading and evapotranspiration is the underlying mechanism of the observed cooling effect [2,6]. The results in Figs. 11 and 12 have strong implications for the mitigation of urban heat stress during hot seasons. For example, the reduced air temperature, surface temperature, and net radiation of ground are beneficial to thermal comfort, especially at the pedestrian level. The decreased wall net radiation and surface temperature also suggest a reduction in the conductive heat flux into buildings, which plays a vital role in building energy saving [8].

5.2 Radiation exchange and turbulent heat fluxes influenced by tree crown radius

We further examine the impacts of varying tree crown radius on urban radiation exchange and turbulent heat fluxes. Similarly, we use input parameters identical to those in Table 3 except for the tree crown size. Here the radius ranges from 0 m (without trees; reference case) to 6 m. Results are shown in Figs. 13 and 14.

Compared to the results in Section 5.1, increasing the tree crown size can more effectively reduce the net radiation of ground and wall via shading. The largest tree crowns (r_T = 6 m) on average reduce the daytime net radiation of ground and wall by 64.80 W m^{-2} and 32.25 W m^{-2}, respectively (compared to the reference case; Fig. 13a and b). The reduction of peak values with increasing tree crown size is nearly linear; for example, the reduction of peak net radiation for ground is ~41.8 W m^{-2} per meter of increase in tree crown radius (R^2 = 0.996). Larger tree crowns can enhance the nighttime radiative trapping effect, leading to greater increases in average net radiation of ground and wall (e.g., an increase of 25.02 W m^{-2} in the average ground net radiation for the case with r_T = 6 m when compared to the reference case). Increasing tree crown radius in general reduces the tree net radiation during the daytime (Fig. 13c). The peak reduction in the tree net radiation occurs in the afternoon, as small tree crowns are strongly affected by the shadow cast by walls. With a constant transmittance, the change of leaf net radiation is proportional to that of tree net radiation (Fig. 13d; see Eqs. (37) and (38)).

The increasing cooling effect of trees with greater tree crown size is also nearly linear (Fig. 14a): a reduction of 0.36 °C in peak canyon air temperature per meter of increase in tree crown radius (R^2 = 0.997). On average, the daytime canyon air temperature for the case with r_T = 6 m is 1.35 °C lower than that for the reference case. The reductions in peak daytime surface temperatures of ground and walls are even greater: 8.87 °C and 6.17 °C, respectively, which are attributable to the shading of trees. The change in nighttime temperatures depends on the tree crown size. For trees with a crown radius lower than 4 m, the radiative trapping effect leads to a higher minimum nighttime air temperature than that in the reference case. But for air temperature in street canyons with bigger tree crowns, the cooling effect dominates its entire diurnal cycle. In contrast, higher ground surface temperatures are found in all cases with trees as compared to the reference case, consistent with field observations in different cities [71,72]. The nighttime warming effect observed here is different from the results using the coupled WRF–ASLUM v3.0 [24,25], primarily because of the simplified tree module (see Section 2) when coupled with the existing WRF-urban modeling system [52]. This highlights that more realistic repartitioning of sensible and latent heat fluxes is of key importance to improve the representation of trees in urban canopy models, as inaccurate repartitioning will likely lead to inaccurate estimates of the cooling effect, especially at night. Urban net radiation shows minor changes with different tree crown sizes (Fig. 14b). As a result of shading and evapotranspiration, the urban sensible heat flux and latent heat flux gradually decreases and increases, respectively, as tree crowns become larger. On the other hand, the increase in latent heat flux gradually plateaus when tree crown radius is greater than 4 m, suggesting that the cooling effect of large trees is mainly attributed to radiative shading.

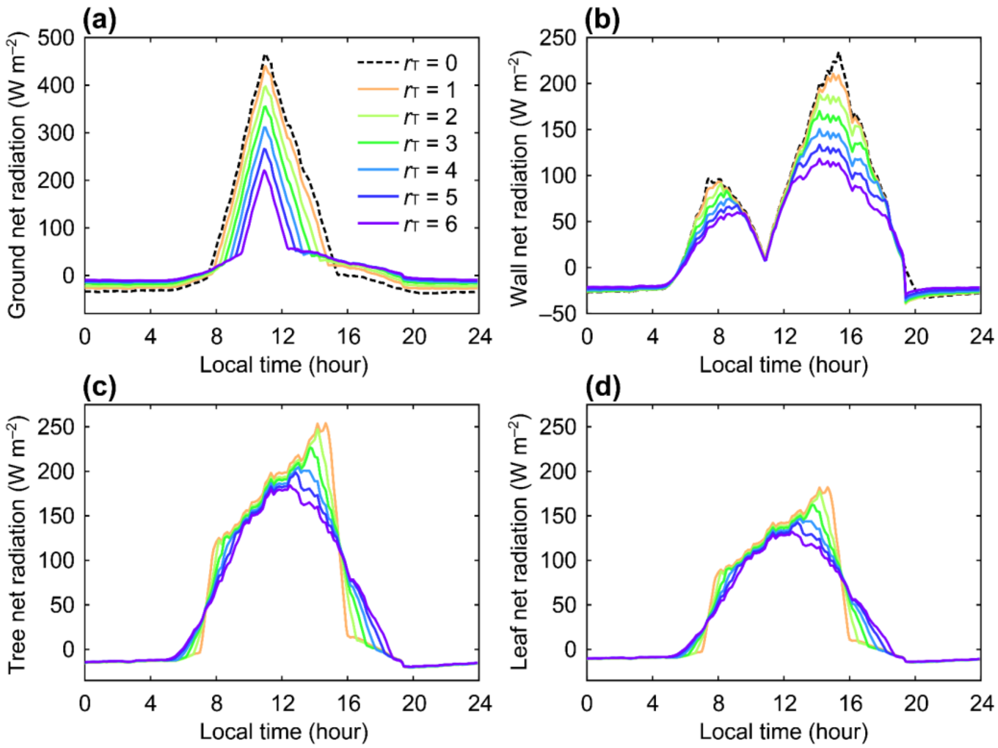

Figure 13. Same as Fig. 11 but with varying tree crown sizes (unit of r_T: m).

(Figure 13 is a 1.5-column fitting image)

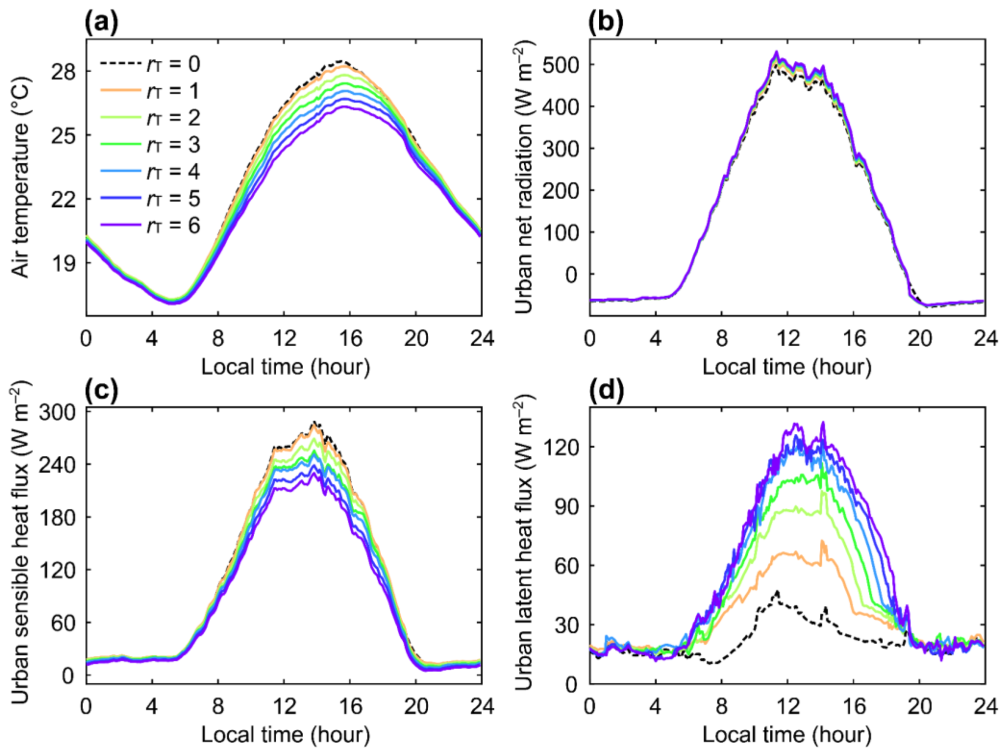

Figure 14. Same as Fig. 12 but with varying tree crown sizes (unit of r_T: m).

(Figure 14 is a 1.5-column fitting image)

6. Concluding remarks

We develop a new Monte Carlo ray tracing method for radiative heat exchange in urban street canyons with trees. The proposed method is able to simulate the impact of canopy transmittance on radiative view factors. Results are evaluated against analytical solutions, suggesting the robustness and accuracy of the proposed model. Sensitivity tests show that the view factors between urban facets and trees are more sensitive to the tree crown size, canyon geometry, and transmittance of foliage, but less sensitive to tree height. This new ray tracing method is then incorporated into a new single-layer urban canopy model (ASLUM v3.1), which enables the realistic numerical representation of radiative shading, evapotranspiration, and root water uptake of urban trees. The performance of ASLUM v3.1 is evaluated against field measurements. Compared to its previous version (ASLUM v2.0), the new urban canopy model exhibits clear improvements in accuracy (especially for latent heat flux). We also apply the model to investigate the effect of trees on radiation exchange, turbulent heat fluxes, and temperatures. Results show that trees with higher LAI and greater crown size can more effectively reduce net radiation of wall and ground, sensible heat flux, and canyon air temperature with enhanced latent heat flux via shading and evapotranspiration, but may exhibit slight warming effect at night due to radiative trapping.

It is noteworthy that for simplicity, the transmittance of urban trees in the proposed model is a lumped parameter based on an empirical equation, and ASLUM v3.1 described here simulates tree evapotranspiration with a few assumptions. The current design in ASLUM v3.1 does not allow trees higher than the buildings. Street canyons with different aspect ratios (especially high aspect ratios) should be evaluated in future applications of the proposed model. The influence of trees on canyon wind and turbulent transport (e.g., [33,41]) is another important component that should be included in future versions of ASLUM. More complex physiological processes of urban trees (e.g., stomatal closure and biogenic carbon exchange [73]) should also be considered in future development for simulations under diverse climate conditions. However, the proposed ray tracing method is sufficiently generic with high accuracy and reliability, so that it can be readily modified to simulate radiation exchange of trees with vertical canopy profiles (e.g., [35,36]) and different shapes (e.g., elliptical or prismatic [74,75]), as well as the impact of airborne pollutants (as participating media [42]) in heavily polluted street canyons. In addition, the proposed ASLUM v3.1 remains simple in its geometry and computationally economic, leaving open the possibility of being incorporated into the WRF platform for online simulations of land–atmosphere interactions. In particular, if seasonal profiles of LAI and transmittance are provided, the new ASLUM v3.1 will enable more realistic simulations of trees with phenological variations. Such simulations can provide critical information in terms of selecting tree species and locations in urban planning through systematic evaluation of how trees affect heat stress, seasonal pedestrian thermal comfort, and building energy consumptions.

Acknowledgements

This work was supported by U.S. National Science Foundation (NSF) under grant # AGS-1930629. The authors would like to acknowledge the use of field observations from the BUBBLE, which was primarily supported by the Swiss Federal Office for Education and Science (Grant C00.0068).

References

[1] D.E. Bowler, L. Buyung-Ali, T.M. Knight, A.S. Pullin, Urban greening to cool towns and cities: A systematic review of the empirical evidence, Landsc. Urban Plan. 97 (2010) 147–155. https://doi.org/10.1016/j.landurbplan.2010.05.006.

[2] S. Hamada, T. Ohta, Seasonal variations in the cooling effect of urban green areas on surrounding urban areas, Urban For. Urban Green. 9 (2010) 15–24. https://doi.org/10.1016/j.ufug.2009.10.002.

[3] S. Gillner, J. Vogt, A. Tharang, S. Dettmann, A. Roloff, Role of street trees in mitigating effects of heat and drought at highly sealed urban sites, Landsc. Urban Plan. 143 (2015) 33–42. https://doi.org/10.1016/j.landurbplan.2015.06.005.

[4] W. Zhou, J. Wang, M.L. Cadenasso, Effects of the spatial configuration of trees on urban heat mitigation: A comparative study, Remote Sens. Environ. 195 (2017) 1–12. https://doi.org/10.1016/j.rse.2017.03.043.

[5] C. Wang, Z.-H. Wang, C.Y. Wang, S.W. Myint, Environmental cooling provided by urban trees under extreme heat and cold waves in U.S. cities, Remote Sens. Environ. 227 (2019) 28–43. https://doi.org/10.1016/j.rse.2019.03.024.

[6] L. Shashua-Bar, D. Pearlmutter, E. Erell, The influence of trees and grass on outdoor thermal comfort in a hot-arid environment, Int. J. Climatol. 31 (2011) 1498–1506. https://doi.org/10.1002/joc.2177.

[7] R. Pandit, D.N. Laband, Energy savings from tree shade, Ecol. Econ. 69 (2010) 1324–1329. https://doi.org/10.1016/j.ecolecon.2010.01.009.

[8] Z.-H. Wang, X. Zhao, J. Yang, J. Song, Cooling and energy saving potentials of shade trees and urban lawns in a desert city, Appl. Energy. 161 (2016) 437–444. https://doi.org/10.1016/j.apenergy.2015.10.047.

[9] H. Akbari, Shade trees reduce building energy use and CO_2 emissions from power plants, Environ. Pollut. 116 (2002) S119–S126. https://doi.org/10.1016/S0269-7491(01)00264-0.

[10] L. Shashua-Bar, M.E. Hoffman, The Green CTTC model for predicting the air temperature in small urban wooded sites, Build. Environ. 37 (2002) 1279–1288. https://doi.org/10.1016/S0360-1323(01)00120-2.

[11] L. Järvi, C.S.B. Grimmond, A. Christen, The Surface Urban Energy and Water Balance Scheme (SUEWS): Evaluation in Los Angeles and Vancouver, J. Hydrol. 411 (2011) 219–237. https://doi.org/10.1016/j.jhydrol.2011.10.001.

[12] V. Masson, A physically-based scheme for the urban energy budget in atmospheric models, Bound.-Layer Meteorol. 94 (2000) 357–397. https://doi.org/10.1023/A:1002463829265.

[13] H. Kusaka, H. Kondo, Y. Kikegawa, F. Kimura, A simple single-layer urban canopy model for atmospheric models: comparison with multi-layer and slab models, Bound.-Layer Meteorol. 101 (2001) 329–358. https://doi.org/10.1023/A:1019207923078.

[14] A. Martilli, A. Clappier, M.W. Rotach, An urban surface exchange parameterization for mesoscale models, Bound.-Layer Meteorol. 104 (2002) 261–304. https://doi.org/10.1023/A:1016099921195.

[15] E.C. Redon, A. Lemonsu, V. Masson, B. Morille, M. Musy, Implementation of street trees within the solar radiative exchange parameterization of TEB in SURFEX v8.0, Geosci. Model Dev. 10 (2017) 385–411. https://doi.org/10.5194/gmd-10-385-2017.

[16] S.-H. Lee, S.-U. Park, A vegetated urban canopy model for meteorological and environmental modelling, Bound.-Layer Meteorol. 126 (2008) 73–102. https://doi.org/10.1007/s10546-007-9221-6.

[17] Z.-H. Wang, Monte Carlo simulations of radiative heat exchange in a street canyon with trees, Sol. Energy. 110 (2014) 704–713. https://doi.org/10.1016/j.solener.2014.10.012.

[18] Y.-H. Ryu, E. Bou-Zeid, Z.-H. Wang, J.A. Smith, Realistic representation of trees in an urban canopy model, Bound.-Layer Meteorol. 159 (2016) 193–220. https://doi.org/10.1007/s10546-015-0120-y.

[19] N. Meili, G. Manoli, P. Burlando, E. Bou-Zeid, W.T.L. Chow, A.M. Coutts, E. Daly, K.A. Nice, M. Roth, N.J. Tapper, E. Velasco, E.R. Vivoni, S. Fatichi, An urban ecohydrological model to quantify the effect of vegetation on urban climate and hydrology (UT&C v1.0), Geosci. Model Dev. 13 (2020) 335–362. https://doi.org/10.5194/gmd-13-335-2020.

[20] E.S. Krayenhoff, A. Christen, A. Martilli, T.R. Oke, A multi-layer radiation model for urban neighbourhoods with trees, Bound.-Layer Meteorol. 151 (2014) 139–178. https://doi.org/10.1007/s10546-013-9883-1.

[21] E.S. Krayenhoff, T. Jiang, A. Christen, A. Martilli, T.R. Oke, B.N. Bailey, N. Nazarian, J.A. Voogt, M.G. Giometto, A. Stastny, B.R. Crawford, A multi-layer urban canopy meteorological model with trees (BEP-Tree): Street tree impacts on pedestrian-level climate, Urban Clim. 32 (2020) 100590. https://doi.org/10.1016/j.uclim.2020.100590.

[22] C.P. Loughner, D.J. Allen, D.-L. Zhang, K.E. Pickering, R.R. Dickerson, L. Landry, Roles of urban tree canopy and buildings in urban heat island effects: Parameterization and preliminary results, J. Appl. Meteorol. Climatol. 51 (2012) 1775–1793. https://doi.org/10.1175/JAMC-D-11-0228.1.

[23] S.-H. Lee, H. Lee, S.-B. Park, J.-W. Woo, D.-I. Lee, J.-J. Baik, Impacts of in-canyon vegetation and canyon aspect ratio on the thermal environment of street canyons: numerical investigation using a coupled WRF-VUCM model, Q. J. R. Meteorol. Soc. 142 (2016) 2562–2578. https://doi.org/10.1002/qj.2847.

[24] R. Upreti, Z.-H. Wang, J. Yang, Radiative shading effect of urban trees on cooling the regional built environment, Urban For. Urban Green. 26 (2017) 18–24. https://doi.org/10.1016/j.ufug.2017.05.008.

[25] C. Wang, Z.-H. Wang, J. Yang, Cooling effect of urban trees on the built environment of contiguous United States, Earth's Future. 6 (2018) 1066–1081. https://doi.org/10.1029/2018EF000891.

[26] G. Mussetti, D. Brunner, S. Henne, J. Allegrini, E.S. Krayenhoff, S. Schubert, C. Feigenwinter, R. Vogt, A. Wicki, J. Carmeliet, COSMO-BEP-Tree v1.0: a coupled urban climate model with explicit representation of street trees, Geosci. Model Dev. 13 (2020) 1685–1710. https://doi.org/10.5194/gmd-13-1685-2020.

[27] Z.-H. Wang, E. Bou-Zeid, J.A. Smith, A coupled energy transport and hydrological model for urban canopies evaluated using a wireless sensor network, Q. J. R. Meteorol. Soc. 139 (2013) 1643–1657. https://doi.org/10.1002/qj.2032.

[28] A. Dimoudi, M. Nikolopoulou, Vegetation in the urban environment: microclimatic analysis and benefits, Energy Build. 35 (2003) 69–76. https://doi.org/10.1016/S0378-7788(02)00081-6.

[29] M. Robitu, M. Musy, C. Inard, D. Groleau, Modeling the influence of vegetation and water pond on urban microclimate, Sol. Energy. 80 (2006) 435–447. https://doi.org/10.1016/j.solener.2005.06.015.

[30] E. Ng, L. Chen, Y. Wang, C. Yuan, A study on the cooling effects of greening in a high-density city: An experience from Hong Kong, Build. Environ. 47 (2012) 256–271. https://doi.org/10.1016/j.buildenv.2011.07.014.

[31] C. Gromke, B. Blocken, W. Janssen, B. Merema, T. van Hooff, H. Timmermans, CFD analysis of transpirational cooling by vegetation: Case study for specific meteorological conditions during a heat wave in Arnhem, Netherlands, Build. Environ. 83 (2015) 11–26. https://doi.org/10.1016/j.buildenv.2014.04.022.

[32] A. Gülten, U.T. Aksoy, H.F. Öztop, Influence of trees on heat island potential in an urban canyon, Sustain. Cities Soc. 26 (2016) 407–418. https://doi.org/10.1016/j.scs.2016.04.006.

[33] M.G. Giometto, A. Christen, P.E. Egli, M.F. Schmid, R.T. Tooke, N.C. Coops, M.B. Parlange, Effects of trees on mean wind, turbulence and momentum exchange within and above a real urban environment, Adv. Water Resour. 106 (2017) 154–168. https://doi.org/10.1016/j.advwatres.2017.06.018.

[34] Z. Wu, L. Chen, Optimizing the spatial arrangement of trees in residential neighborhoods for better cooling effects: Integrating modeling with in-situ measurements, Landsc. Urban Plan. 167 (2017) 463–472. https://doi.org/10.1016/j.landurbplan.2017.07.015.

[35] Q. Li, Z.-H. Wang, Large-eddy simulation of the impact of urban trees on momentum and heat fluxes, Agric. For. Meteorol. 255 (2018) 44–56. https://doi.org/10.1016/j.agrformet.2017.07.011.

[36] C. Wang, Q. Li, Z.-H. Wang, Quantifying the impact of urban trees on passive pollutant dispersion using a coupled large-eddy simulation–Lagrangian stochastic model, Build. Environ. 145 (2018) 33–49. https://doi.org/10.1016/j.buildenv.2018.09.014.

[37] M. Fahmy, S. Sharples, On the development of an urban passive thermal comfort system in Cairo, Egypt, Build. Environ. 44 (2009) 1907–1916. https://doi.org/10.1016/j.buildenv.2009.01.010.

[38] N. Müller, W. Kuttler, A.-B. Barlag, Counteracting urban climate change: adaptation measures and their effect on thermal comfort, Theor. Appl. Climatol. 115 (2014) 243–257. https://doi.org/10.1007/s00704-013-0890-4.

[39] C.S.B. Grimmond, M. Blackett, M.J. Best, J.-J. Baik, S.E. Belcher, J. Beringer, S.I. Bohnenstengel, I. Calmet, F. Chen, A. Coutts, A. Dandou, K. Fortuniak, M.L. Gouvea, R. Hamdi, M. Hendry, M. Kanda, T. Kawai, Y. Kawamoto, H. Kondo, E.S. Krayenhoff, S.-H. Lee, T. Loridan, A. Martilli, V. Masson, S. Miao, K. Oleson, R. Ooka, G. Pigeon, A. Porson, Y.-H. Ryu, F. Salamanca, G.J. Steeneveld, M. Tombrou, J.A. Voogt, D.T. Young, N. Zhang, Initial results from Phase 2 of the international urban energy balance model comparison, Int. J. Climatol. 31 (2011) 244–272. https://doi.org/10.1002/joc.2227.

[40] C.S.B. Grimmond, M. Blackett, M.J. Best, J. Barlow, J.-J. Baik, S.E. Belcher, S.I. Bohnenstengel, I. Calmet, F. Chen, A. Dandou, K. Fortuniak, M.L. Gouvea, R. Hamdi, M. Hendry, T. Kawai, Y. Kawamoto, H. Kondo, E.S. Krayenhoff, S.-H. Lee, T. Loridan, A. Martilli, V. Masson, S. Miao, K. Oleson, G. Pigeon, A. Porson, Y.-H. Ryu, F. Salamanca, L. Shashua-Bar, G.-J. Steeneveld, M. Tombrou, J. Voogt, D. Young, N. Zhang, The international urban energy balance models comparison project: First results from Phase 1, J. Appl. Meteorol. Climatol. 49 (2010) 1268–1292. https://doi.org/10.1175/2010JAMC2354.1.

[41] E. Redon, A. Lemonsu, V. Masson, An urban trees parameterization for modeling microclimatic variables and thermal comfort conditions at street level with the Town

Energy Balance model (TEB-SURFEX v8.0), Geosci. Model Dev. 13 (2020) 385–399. https://doi.org/10.5194/gmd-13-385-2020.

[42] J.R. Howell, M.P. Mengüç, R. Siegel, Thermal Radiation Heat Transfer, 6 edition, CRC Press, Boca Raton, FL, 2016.

[43] D.T. Young, P. Clark, M. Hendry, J. Barlow, Modelling radiative exchange in a vegetated urban street canyon model, 9th International Conference on Urban Climate jointly with 12th Symposium on the Urban Environment, Toulouse, France, 2015.

[44] Z.-H. Wang, E. Bou-Zeid, S.K. Au, J.A. Smith, Analyzing the sensitivity of WRF's single-layer urban canopy model to parameter uncertainty using advanced Monte Carlo simulation, J. Appl. Meteorol. Climatol. 50 (2011) 1795–1814. https://doi.org/10.1175/2011JAMC2685.1.

[45] K.W. Oleson, G.B. Bonan, J. Feddema, M. Vertenstein, C.S.B. Grimmond, An urban parameterization for a global climate model. Part I: formulation and evaluation for two cities, J. Appl. Meteorol. Climatol. 47 (2008) 1038–1060. https://doi.org/10.1175/2007JAMC1597.1.

[46] Z.-H. Wang, E. Bou-Zeid, J.A. Smith, A spatially-analytical scheme for surface temperatures and conductive heat fluxes in urban canopy models, Bound.-Layer Meteorol. 138 (2011) 171–193. https://doi.org/10.1007/s10546-010-9552-6.

[47] Z.-H. Wang, E. Bou-Zeid, A novel approach for the estimation of soil ground heat flux, Agric. For. Meteorol. 154–155 (2012) 214–221. https://doi.org/10.1016/j.agrformet.2011.12.001.

[48] Z.-H. Wang, Reconstruction of soil thermal field from a single depth measurement, J. Hydrol. 464–465 (2012) 541–549. https://doi.org/10.1016/j.jhydrol.2012.07.047.

[49] T. Sun, E. Bou-Zeid, Z.-H. Wang, E. Zerba, G.-H. Ni, Hydrometeorological determinants of green roof performance via a vertically-resolved model for heat and water transport, Build. Environ. 60 (2013) 211–224. https://doi.org/10.1016/j.buildenv.2012.10.018.

[50] J. Yang, Z.-H. Wang, F. Chen, S. Miao, M. Tewari, J.A. Voogt, S. Myint, Enhancing hydrologic modelling in the coupled weather research and forecasting–urban modelling system, Bound.-Layer Meteorol. 155 (2015) 87–109. https://doi.org/10.1007/s10546-014-9991-6.

[51] J. Yang, Z.-H. Wang, Physical parameterization and sensitivity of urban hydrological models: Application to green roof systems, Build. Environ. 75 (2014) 250–263. https://doi.org/10.1016/j.buildenv.2014.02.006.

[52] F. Chen, H. Kusaka, R. Bornstein, J. Ching, C.S.B. Grimmond, S. Grossman-Clarke, T. Loridan, K.W. Manning, A. Martilli, S. Miao, D. Sailor, F.P. Salamanca, H. Taha, M. Tewari, X. Wang, A.A. Wyszogrodzki, C. Zhang, The integrated WRF/urban modelling system: development, evaluation, and applications to urban environmental problems, Int. J. Climatol. 31 (2011) 273–288. https://doi.org/10.1002/joc.2158.

[53] J. Song, Z.-H. Wang, C. Wang, The regional impact of urban heat mitigation strategies on planetary boundary-layer dynamics over a semiarid city, J. Geophys. Res. Atmospheres. 123 (2018) 6410–6422. https://doi.org/10.1029/2018JD028302.

[54] J. Yang, Z.-H. Wang, M. Georgescu, F. Chen, M. Tewari, Assessing the impact of enhanced hydrological processes on urban hydrometeorology with application to two cities in contrasting climates, J. Hydrometeorol. 17 (2016) 1031–1047. https://doi.org/10.1175/JHM-D-15-0112.1.

[55] W.C. Skamarock, J.B. Klemp, J. Dudhia, D.O. Gill, D.M. Barker, M.G. Duda, X.-Y. Huang, W. Wang, J.G. Powers, A Description of the Advanced Research WRF Version 3 (No. NCAR/TN-475+STR), University Corporation for Atmospheric Research, 2008. https://doi.org/10.5065/D68S4MVH.

[56] J. Song, Z.-H. Wang, Interfacing the urban land–atmosphere system through coupled urban canopy and atmospheric models, Bound.-Layer Meteorol. 154 (2015) 427–448. https://doi.org/10.1007/s10546-014-9980-9.

[57] I.N. Harman, M.J. Best, S.E. Belcher, Radiative exchange in an urban street canyon, Bound.-Layer Meteorol. 110 (2004) 301–316. https://doi.org/10.1023/A:1026029822517.

[58] A. Feingold, K.G. Gupta, New analytical approach to the evaluation of configuration factors in radiation from spheres and infinitely long cylinders, J. Heat Transf. 92 (1970) 69–76. https://doi.org/10.1115/1.3449647.

[59] A. Frank, W. Heidemann, K. Spindler, Modeling of the surface-to-surface radiation exchange using a Monte Carlo method, J. Phys. Conf. Ser. 745 (2016) 032143. https://doi.org/10.1088/1742-6596/745/3/032143.

[60] P.G. Jarvis, J.W. Leverenz, Productivity of Temperate, Deciduous and Evergreen Forests, in: O.L. Lange, P.S. Nobel, C.B. Osmond, H. Ziegler (Eds.), Physiological Plant Ecology IV: Ecosystem Processes: Mineral Cycling, Productivity and Man’s Influence, Springer, Berlin, Heidelberg, 1983: pp. 233–280. https://doi.org/10.1007/978-3-642-68156-1_9.

[61] N.J.J. Bréda, Ground-based measurements of leaf area index: a review of methods, instruments and current controversies, J. Exp. Bot. 54 (2003) 2403–2417. https://doi.org/10.1093/jxb/erg263.

[62] J.M. Welles, S. Cohen, Canopy structure measurement by gap fraction analysis using commercial instrumentation, J. Exp. Bot. 47 (1996) 1335–1342. https://doi.org/10.1093/jxb/47.9.1335.

[63] J. Maass, J.M. Vose, W.T. Swank, A. Martínez-Yrízar, Seasonal changes of leaf area index (LAI) in a tropical deciduous forest in west Mexico, For. Ecol. Manag. 74 (1995) 171–180. https://doi.org/10.1016/0378-1127(94)03485-F.

[64] J. Konarska, F. Lindberg, A. Larsson, S. Thorsson, B. Holmer, Transmissivity of solar radiation through crowns of single urban trees—application for outdoor thermal comfort modelling, Theor. Appl. Climatol. 117 (2014) 363–376. https://doi.org/10.1007/s00704-013-1000-3.

[65] S.R. Green, Radiation balance, transpiration and photosynthesis of an isolated tree, Agric. For. Meteorol. 64 (1993) 201–221. https://doi.org/10.1016/0168-1923(93)90029-H.

[66] H. Sinoquet, X.L. Roux, Short term interactions between tree foliage and the aerial environment: An overview of modelling approaches available for tree structure-function models, Ann. For. Sci. 57 (2000) 477–496. https://doi.org/10.1051/forest:2000136.

[67] N.J. Jarvis, A simple empirical model of root water uptake, J. Hydrol. 107 (1989) 57–72. https://doi.org/10.1016/0022-1694(89)90050-4.

[68] M.W. Rotach, R. Vogt, C. Bernhofer, E. Batchvarova, A. Christen, A. Clappier, B. Feddersen, S.-E. Gryning, G. Martucci, H. Mayer, V. Mitev, T.R. Oke, E. Parlow, H. Richner, M. Roth, Y.-A. Roulet, D. Ruffieux, J.A. Salmond, M. Schatzmann, J.A. Voogt, BUBBLE – an urban boundary layer meteorology project, Theor. Appl. Climatol. 81 (2005) 231–261. https://doi.org/10.1007/s00704-004-0117-9.

[69] Y.-H. Ryu, J.-J. Baik, S.-H. Lee, A new single-layer urban canopy model for use in mesoscale atmospheric models, J. Appl. Meteorol. Climatol. 50 (2011) 1773–1794. https://doi.org/10.1175/2011JAMC2665.1.

[70] L. Shashua-Bar, I.X. Tsiros, M. Hoffman, Passive cooling design options to ameliorate thermal comfort in urban streets of a Mediterranean climate (Athens) under hot summer conditions, Build. Environ. 57 (2012) 110–119. https://doi.org/10.1016/j.buildenv.2012.04.019.

[71] A.M. Coutts, E.C. White, N.J. Tapper, J. Beringer, S.J. Livesley, Temperature and human thermal comfort effects of street trees across three contrasting street canyon environments, Theor. Appl. Climatol. 124 (2016) 55–68. https://doi.org/10.1007/s00704-015-1409-y.

[72] C.A. Souch, C. Souch, The effect of trees on summertime below canopy urban climates: A case study Bloomington, Indiana, J. Arboric. 19 (1993) 303–312.

[73] T.T. Kozlowski, P.J. Kramer, S.G. Pallardy, The Physiological Ecology of Woody Plants, Academic Press, San Diego, California, 1991. https://doi.org/10.1016/C2009-0-02706-8.

[74] G.S. Campbell, Extinction coefficients for radiation in plant canopies calculated using an ellipsoidal inclination angle distribution, Agric. For. Meteorol. 36 (1986) 317–321. https://doi.org/10.1016/0168-1923(86)90010-9.

[75] R.A. Oyarzun, C.O. Stöckle, M.D. Whiting, A simple approach to modeling radiation interception by fruit-tree orchards, Agric. For. Meteorol. 142 (2007) 12–24. https://doi.org/10.1016/j.agrformet.2006.10.004.